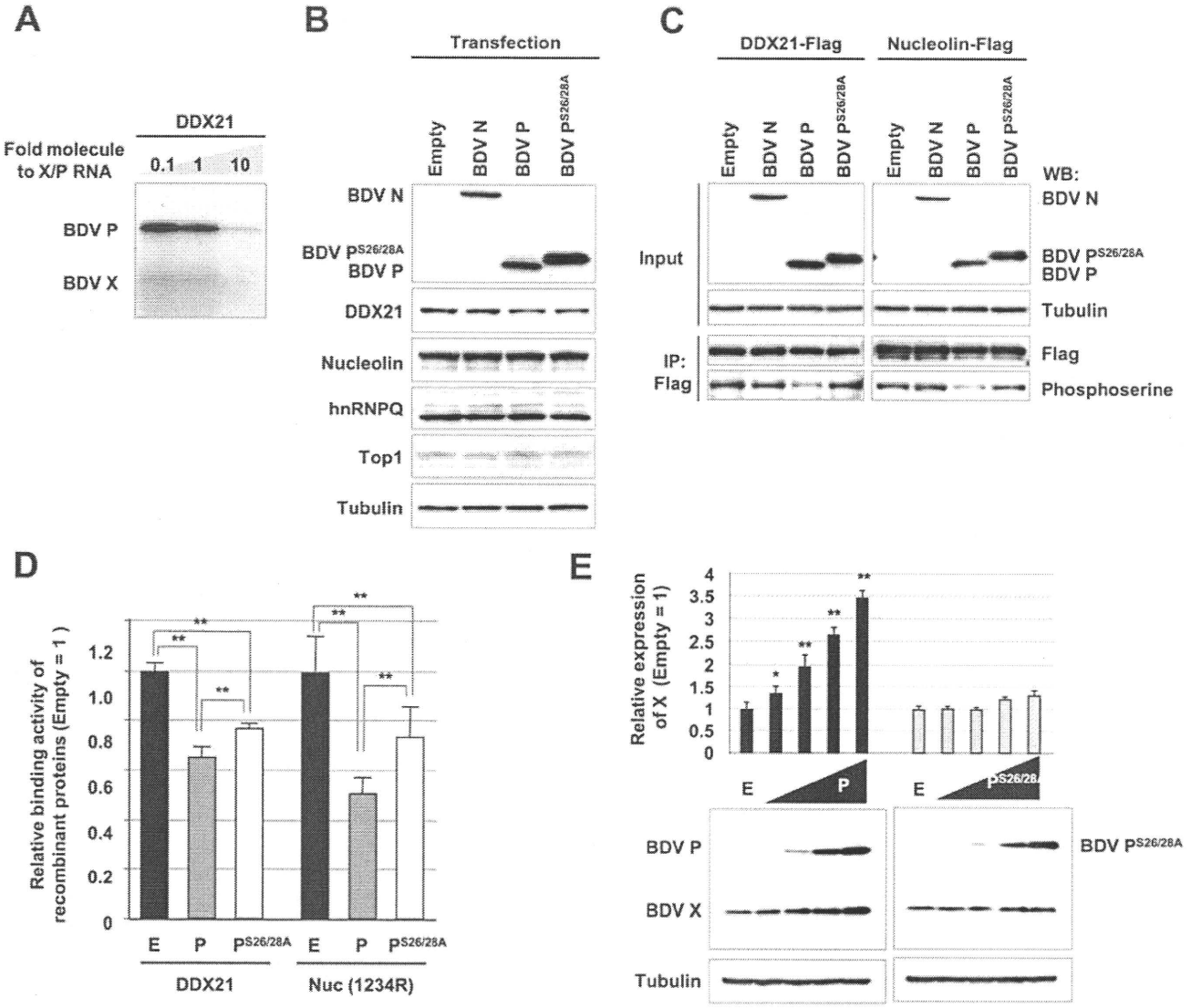

Figure 9. Interaction between BDV P phosphorylation and translation of the X ORF. (A) *In vitro* RNA binding and translation assay of DDX21 and X/P mRNA. *In vitro* transcribed X/P mRNA was incubated with recombinant DDX21 and then *in vitro* translation was performed using a rabbit reticulocyte lysate, according to the manufacturer's recommendations. After incubation, 10 μl of the mixture was subjected to SDS-PAGE and Western blotting using anti-P and -X antibodies. (B) BDV P does not influence the expression of UBPs. OL cells were transfected with plasmids expressing BDV N, P or $P^{S26/28A}$, and 48 h post-transfection the cells were lysed with sample buffer and then subjected to Western blotting using the antibodies indicated. (C) Expression of P reduces phosphorylation levels of DDX21 and nucleolin. Flag-tagged DDX21 or nucleolin was cotransfected with BDV N, P or $P^{S26/28A}$ into OL cells. Forty-eight h after transfection, the cell lysates were immunoprecipitated by anti-Flag antibody and the immunoprecipitants were detected by anti-Flag and anti-phosphoserine antibodies. (D) Expression of P reduces the RNA-binding activity of DDX21 and nucleolin. Flag-tagged recombinant DDX21 and nucleolin were obtained from lysates of OL cells transfected with either empty (E), wt P (P) or mutant P ($P^{S26/28A}$) expression plasmid, and *in vitro* RNA binding assay was performed with ^{32}P-labeled X/P UTR riboprobe and purified recombinant proteins as described in the Methods section. Each value represents the mean plus S.D. of at least three independent experiments. $^{**}P<0.01$, (Student's *t* test). (E) BDV P, but not the $P^{S26/28A}$ mutant, enhances translation of X ORF. OL cells were cotransfected with 0.4 g of pX/PΔP and a serially diluted P or $P^{S26/28A}$ plasmid (4 fold dilution; 0.00625, 0.025, 0.1, 0.4 μg). The expression of BDV X, P and $P^{S26/28A}$ was detected by Western blotting. The relative expression level of X is shown. Each value represents the mean plus S.D. of three independent experiments. E: empty plasmid-transfected. $^{**}P<0.01$, $^{*}P<0.05$ (Student's *t* test).
doi:10.1371/journal.ppat.1000654.g009

nonspecific inhibition of the translation of other mRNAs (data not shown). Therefore, we sought to investigate further the effect of DDX21 on the translation of the X ORF by focusing on its interaction with P. P is phosphorylated and acts as a protein kinase substrate, inhibiting the phosphorylation of host proteins to modify their functions [39,40]. A recent study demonstrated the phosphorylation of DDX21 [41]. Furthermore, the phosphorylation of RNA helicases, such as nucleolin, is known to be critical for RNA-binding activity [42]. Therefore, it is tempting to speculate that interference with phosphorylation by P affects the ability of DDX21 to bind to the X/P UTR. To address this, we examined whether the phosphorylation of DDX21 is affected by the expression of P. OL cells were transfected with wt or mutant P, $P^{S26/28A}$, in which two major phosphorylation sites (Ser26, Ser28) were substituted by alanine [39,43], and the phosphorylation of DDX21, as well as nucleolin, was monitored. Although the

expression levels of the UBPs were unchanged by the expression of P (Figure 9B), the phosphorylation levels of both DDX21 and nucleolin decreased clearly in the cells transfected with wt P, but not with $P^{S26/28A}$ (Figure 9C).

To investigate whether the hypophosphorylation of DDX21 in the presence of P modulates its RNA binding activity, we extracted Flag-tagged DDX21 from the cells transfected with wt P or $P^{S26/28A}$ and then estimated its binding ability to the ^{32}P-labelled X/P UTR probe using an *in vitro* RNA binding assay. As shown in Figure 9D, Flag-tagged DDX21, as well as nucleolin, from wt P-transfected cells exhibited significant reduction of binding to X/P UTR. The binding activities of the tagged proteins from the cells transfected with $P^{S26/28A}$ were significantly higher than those with wt P, suggesting that interference with phosphorylation by P decreases the RNA binding activity of DDX21. Therefore, we finally examined whether phosphorylation of P directly affects translation of the X ORF. Consistent with Figure 3B, the expression of X was significantly upregulated in the pX/PΔP-transfected cells in the presence of wt P in a dose-dependent fashion, whereas the $P^{S26/28A}$ mutant was not able to upregulate the translation of X (Figure 9E). Altogether, these results suggested that BDV P may inhibit the binding of DDX21 to the 5′ UTR by interfering with its phosphorylation, resulting in the upregulation of the ribosomal reinitiation from the X-AUG.

Discussion

In this study, we demonstrated translational regulation of polycistronic mRNA in a unique animal RNA virus. The BDV X/P polycistronic mRNA encodes three overlapping ORFs within a short, 0.8 kb sequence. We showed that the X and P ORFs are translated predominantly by a reinitiation strategy, following the termination of translation of the uORF, although a leaky scanning mechanism is implicated to some extent in the translational processes. In this study, we employed an RNA polymerase II-controlled vector for expression of the X/P mRNA in transfected cells. We have carefully investigated the expression, as well as the structure, of the transcripts from pX/P plasmid DNAs in each experiment and then verified that our system could recreate the translational regulation of X/P mRNA in BDV-infected cells (data not shown). Currently, two types of reinitiation mechanism have been identified in eukaryotic and viral mRNAs [2,3,6,11,17,18]. The first type of mRNAs contain short uORFs (<30 codons) upstream of the main ORFs. In this mechanism, the efficiency of reinitiation is controlled by the length of the uORF and by the intercistronic region, an appropriate distance being necessary for the recharging of reinitiation factors, including eIF2 and Met-tRNAiMet, to the ribosomes. Cellular mRNAs such as C/EBP and AdoMetDC, are representative examples of this type of regulation [17,44]. In the X/P mRNA, initiation of translation of the P ORF may be mediated by this type of reinitiation mechanism. The scanning ribosomes, which travel continuously on the mRNA after termination of translation of the uORF, must recharge the initiation factors on the intercistronic region between the uORF and P ORF and efficiently initiate translation from the P-AUG. Note that the expression level of P is quite invariant, with or without translation of X, if the uORF is present (Figure 2), indicating that the number of ribosomes, which move continuously along the mRNA after uORF termination, is relatively constant on the X/P mRNA. This may be the mechanism underlying the stable and persistent expression of P in infected cells.

The second type of reinitiation mechanism involves mRNAs containing long 5′ ORFs, which usually encode functional proteins. These mRNAs display only short intercistronic distances between the upstream and downstream ORFs, or even may overlap. It has been shown that efficient reinitiation in this mechanism is determined by the stability/mobility of ribosomal complexes to allow reinitiation at the downstream initiation codon [17,18]. Among viral mRNAs, segment 7 of influenza B virus [45], the ORF-2 of the M2 gene of respiratory syncytial virus (RSV) [46], and the 3′ terminal ORF (VP2) of feline calicivirus (FCV) [47,48] represent are examples of this type of reinitiation process. Our experiments revealed that reinitiation of the X ORF may be regulated by this type of mechanism, although the uORF encodes only a short and, probably, non-functional peptide. Interestingly, the uORF and X ORF feature an overlapping stop-start codon, UGAUG, as found in other viral polycistronic mRNAs [47,49,50]. This feature indicates that the overlapping stop-start codon of the X/P mRNA may play a key role in the regulation of translation of the X ORF. Previous studies revealed that genes divided by such an overlapping stop-start codon are expressed predominantly by termination-coupled translation, in which translation of the downstream ORF is initiated by ribosomes which have read the uORF and stalled at the overlapping stop-start codon [48,51]. The downstream extension of the termination signal of the uORF in the X/P mRNA significantly reduced the expression of X, suggesting that ribosomal reinitiation from the X-AUG is also carried out by the coupled translation mechanism associated with uORF termination.

The regulation of ribosomal movement/stability around the overlapping stop-start codon must be crucial for controlling the translation of the downstream ORF. The scanning ribosomes, which have not dissociated from the mRNA after stalling at the uORF termination codon, may be reutilized efficiently for the reinitiation of translation of the X ORF. In favor of this hypothesis, we found that host nuclear factors influence ribosomal initiation of the X ORF through interaction with the 5′ UTR and identified RNA helicase complexes, mainly involving DDX21. DDX21 is a DEAD-box RNA helicase that localizes to the nucleoli and is involved in ribosomal RNA synthesis or processing [38,52,53]. Although detailed functions of DDX21 have not been elucidated yet, this helicase appears to fold or unwind RNA or ribonucleoprotein structures through regulation of RNA-RNA or RNA-protein interaction [38,52,53]. We found that DDX21 may be a scaffold protein that interacts with the X/P UTR, among the UBPs, and causes structural alteration of the 5′ UTR. Numerous reports have demonstrated that RNA secondary structure contributes to translational control by affecting the constancy of ribosomal scanning on mRNAs or the recognition of initiation signals [6,54]. The ribosomes may stack or pass through the initiation codons if secondary structures are formed around the initiation site, leading to enhancement or reduction of the translation efficiency of the ORFs. Therefore, it is conceivable that structural modification of the X/P UTR by DDX21 and the UBPs decreases the ribosomal reinitiation at the X ORF or increases ribosomal dissociation from the mRNA after termination of translation of the uORF, both resulting in the suppression of the translation of the X ORF (Figure 10, left arrow). We found that the structural alterations induced by the base-pair changes in a short stem-loop structure within the X/P UTR influence the translation of the X ORF (Figure S8), supporting this conclusion. On the other hand, in this model the structural change of the X/P UTR should occur in the cytoplasm. Considering DDX21 is mostly a nuclear protein [53], it is possible that the transient interaction of DDX21 with X/P mRNA in the nucleus is enough to maintain the structure of X/P UTR in the cytoplasm by introducing the UBPs (Figure 10, left arrow). Alternatively, DDX21 may be transported to the cytoplasm along with the mRNA in this case.

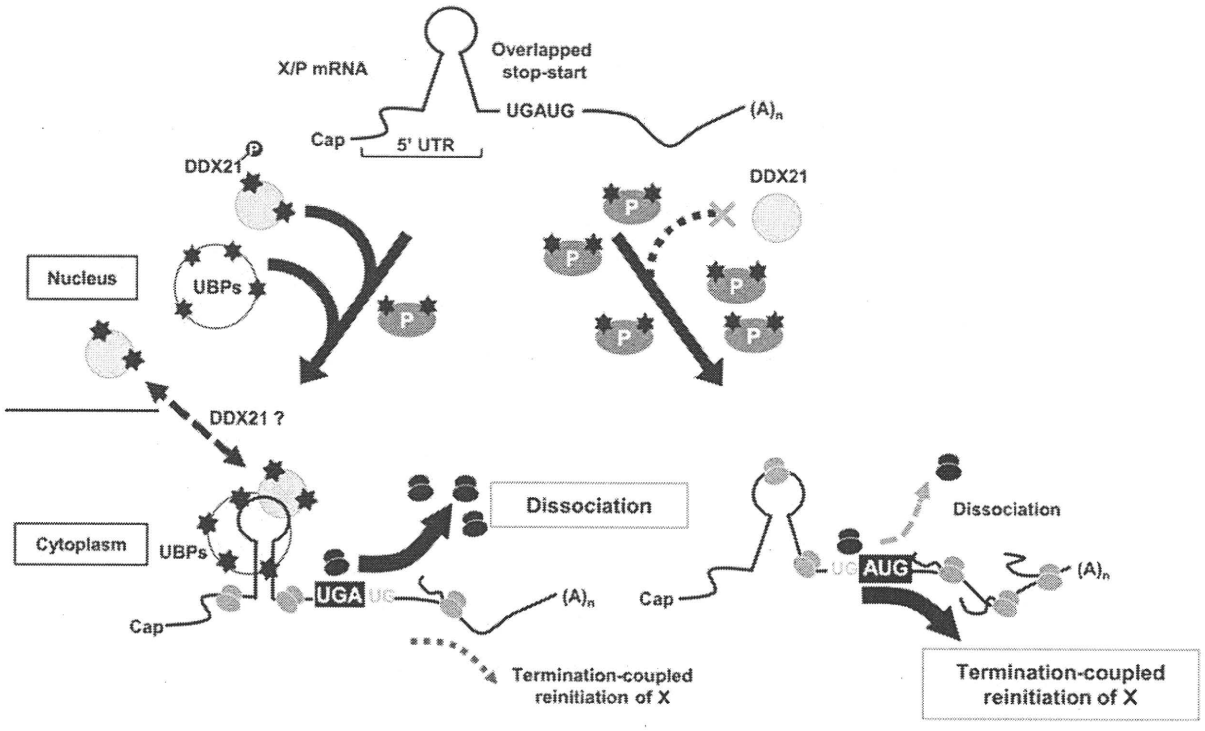

Figure 10. Possible mechanism of autogenous regulation of BDV polycistronic mRNA translation. During the early stage of BDV replication, the phosphorylated DDX21 and other UBPs, including nucleolin, interact with the 5′ UTR of X/P mRNA (left arrow). The interaction may facilitate dissociation or impede X-AUG recognition of ribosomes at the overlapping stop-start codon, leading to inefficient termination-coupled reinitiation, by ribosomes which have translated the uORF, at the X ORF. The DDX21 may be dissociated from the 5′ UTR in the cytoplasm. BDV P accumulation in BDV-infected cells may interfere with phosphorylation of DDX21 and UBPs (right arrow), resulting in the detachment of the RNA helicase complex from the 5′ UTR. The free 5′ UTR may increase the reinitiation processes of ribosomes at X-AUG.
doi:10.1371/journal.ppat.1000654.g010

We revealed that phosphorylation of DDX21, as well as nucleolin, is inhibited by expression of P. Previous studies demonstrated that hyperphosphorylation of nucleolin increases its RNA binding affinity, whereas dephosphorylation reduces the affinity [42]. In this study, the RNA-binding activity of DDX21 was shown to be reduced significantly in cells expressing P. These data suggested that accumulation of P in infected cells blocks interaction of DDX21 with the X/P UTR, resulting in upregulation of translation of the X ORF by promotion of ribosomal reinitiation (Figure 10, right arrow). Note that in Figure 9D the $P^{S26/28A}$ did not fully recover the binding activity of DDX21 to the X/P UTR. This suggests that hypophosphorylation of DDX21 may be not exclusively involved in the promotion of the translation of X, although the *in vitro* binding assay based on the transfection may be insensitive for the detection of the binding activity of DDX21 to the 5′ UTR.

Previous studies showed that the intranuclear stoichiometry of N and P is important for BDV polymerase activity and that accumulation of P in the nucleus markedly disturbs both viral replication and persistent infection [21,55,56]. Interestingly, it has been demonstrated that X binds directly to P and promotes translocation of P to the cytoplasm from the nucleus [30,33]. Therefore, P-dependent translational regulation of X must be a convenient and effective mechanism for ensuring an optimal level of P in the nucleus. The nuclear accumulation of P above the threshold level upregulates the translation of X, thereby leading to the translocation of P to the cytoplasm. This could keep the amount of P at the optimal level in the nucleus, which is unequivocally necessary for productive replication and/or persistent infection of BDV in the nucleus. A previous study, which demonstrated that the mutations in Ser26 and Ser28 of P aberrantly upregulate the viral polymerase complex activity, and that recombinant BDVs containing the phosphorylation mutations (rBDV-$P^{S26/28A}$) reduce the expression of X in infected cells [43], may be consistent with our findings, although the possibility that two amino acid changes inevitably introduced in the X ORF of rBDV-$P^{S26/28A}$ affect the expression level of X has remained. In addition, a recent work using a mutant rBDV, which ectopically expresses X under the different transcriptional unit, demonstrated that the expression of X from the mutant virus is not as tightly linked to expression of P as in the wild type BDV, resulting in strong attenuation of the replication of the rBDV in rat brains [57]. This observation may also support our conclusion that the X/P UTR is not only specifically involved in the regulational expression of X but also essentially controls the balanced expression between X and P in infected cells. Furthermore, a recent work by Poenisch et al. [31] showed that recombinant BDVs containing either a premature stop codon in the uORF or mutations ablating the stop codons of the uORF express wild-type like X and P in cultured cells and efficiently replicate in the brains of adult rats. Although this observation may seem to conflict with our findings that the overlapped termination of uORF is critical for the translation reinitiation of X, the recombinant viruses may be able to recover the translation level of X by the expression of other transcription unit, such as a 1.9-kb mRNA, resulting in the efficient replication in infected cells. In fact, Poenisch et al. [31] have demonstrated that the 1.9-kb mRNA not only serves as a template for the synthesis of N but also might be used for the translation of the viral P protein and possibly X, suggesting that the 1.9-kb transcript is a multicistronic mRNA of BDV.

This is the first example, to our knowledge, of autogenous translational regulation of polycistronic mRNA mediated by its own encoding protein and host RNA helicases. The detailed description of the mechanism should provide novel insights into not only an ingenious strategy of virus replication but also the roles of RNA helicases in the translation of eukaryotic mRNAs. Further study remains to be done to discover cellular mRNAs using a similar translation strategy.

Materials and Methods

Cell culture and virus

The COS-7 cell line was grown in Dulbecco's modified Eagle's medium (DMEM) supplemented with 5% heat-inactivated fetal calf serum (FCS) at 37°C in a humidified atmosphere of 95% air and 5% CO2. The OL cell line, derived from a human oligodendroglioma, was grown in high-glucose (4.5%) DMEM supplemented with 5% FCS. Cells were passaged every 3 days. The BDV strain huP2br [32,58] was used for analyses in this study.

Plasmids

Construction of the expression plasmids for BDV X/P mRNA, N, P and P phosphorylation mutants has been described elsewhere [29,30,32,33,39,43]. The mutant forms of the plasmids were generated using PCR-based site-directed mutagenesis. To generate X/P-Luciferase hybrid mRNAs, a luciferase gene was fused in frame with the X and P ORFs at the 148 nt and 149 nt positions of the coding sequences, respectively, and introduced into the pcDNA3 vector (Invitrogen) at the *Kpn* I-*Not* I sites. The first AUG codon of Luc was replaced by AAG. For expression of DDX21, DDX50, nucleolin, TOP1 and hnRNPQ1, corresponding cDNAs were amplified by RT-PCR from OL cells and inserted into pcXN2, pET32a or pET42a vectors (Novagen). Cells were transfected with equimolar ratios of plasmid DNAs using Lipofectamine™ 2000 (Invitrogen) or FuGENE6 (Roche Applied Science), according to the manufacturer's instructions, and cellular samples were collected at the desired times. The introduction of the correct sequences for the wild type and its mutant were confirmed by DNA sequencing and Western blotting analysis of protein production.

To generate glutathione S-transferase (GST)-tagged DDX21 and nucleolin recombinant proteins used in the Escherichia coli system, we cloned the amplified cDNAs into the pET42a vector (Novagen). The vectors were transformed into BL21 (DE3) (Novagen), and the expression of the GST-tagged proteins was induced by the addition of 0.3 mM IPTG. The cell pellets were resuspended in PBS(-) and then lysed by sonication. After centrifugation, the supernatants were loaded on glutathione sepharose 4B (Amersham Biosciences). Eluted proteins were concentrated using Centricon spin columns (Millipore Corporation) and dialyzed against a 20 mM HEPES (pH 7.5)-100 mM KCl buffer.

The His-tagged DDX21 was generated by the insertion of the PCR-based DDX21 cDNA into PET32a vector (Novagen) and the resultant plasmid was transformed into Rosetta-gami B(De3)pLysS competent cells (Novagen). Purification of the recombinant DDX21 using Ni-NTA agarose (QIAGEN) was performed according to the manufacturer's recommendations.

Luciferase reporter assay

COS-7 and OL cells cultured in 12-well plates were transfected with plasmids expressing X/P-Luc hybrid mRNA. At 6 h post-transfection, cells were lysed and subjected to luciferase assay system (Promega Corporation), according to the manufacturer's recommendations. The relative levels of luciferase activity were calculated for each fusion plasmid.

Western blot and immunoprecipitation analyses

For Western blotting, equal amounts of total lysate proteins of COS-7 or OL cells transfected with expression plasmids were subjected to SDS-PAGE and transferred onto polyvinylidene difluoride membrane (Millipore Corporation). Antibodies used in this study were as follows: anti-BDV P mouse monoclonal, anti-BDV X rabbit polyclonal antibodies [30,33], mouse anti-Flag M2 (Sigma-Aldrich), mouse anti-HA 12CA5 (Roche Applied Science), rabbit DDX21 (Bethyl Laboratories), rabbit Nucleolin (Novus Biologicals), rabbit anti-Topo1 (TopGEN, Inc), mouse hnRNP-Q (ImmunoQuest Ltd), rabbit anti-phosphoserine (ZYMED Laboratories).

For immunoprecipitation (IP) assay, OL cells transfected with Flag-tagged plasmids were lysed with RIPA buffer [20 mM Tris-HCl (pH 7.4), 150 mM NaCl, 2 mM EDTA, 1% Nonidet P-40 (NP-40), 1% Na-deoxycholate with protease inhibitors]. After centrifugation at 15,000 rpm for 30 min, the supernatants were incubated with 40 µl of pre-equilibrated anti-Flag M2 agarose (Sigma-Aldrich) overnight at 4°C with gentle rotation. After incubation, beads were collected by centrifugation at 6,000 rpm for 40 s and washed four times with 1 ml of RIPA. The proteins immunoprecipitated with anti-Flag agarose were eluted with 3×Flag peptide (Sigma-Aldrich) in RIPA buffer and detected by Western blotting as described above. In IP for detection of phosphoserine, NaF and Na3VO4 were added in RIPA buffer, and the serine-phosphorylated proteins were detected by anti-phosphoserine antibody.

IP-RT-PCR

To detect the interaction of host factors with BDV X/P mRNA *in vivo*, BDV-infected OL cells were transfected with Flag-tagged targeted proteins and lysed with RIPA buffer with RNasin (Promega). After IP with anti-Flag M2, the co-immunoprecipitants were boiled in TE buffer and then treated with RNase-free DNase I for 20 min. Total RNAs were isolated from the aqueous solution and used as templates for RT-PCR using specific primers of X/P mRNA.

In vitro translation assay

In vitro transcribed X/P-Luc mRNAs were prepared with Maxiscript Kits (Ambion). About 1.0 pmol of X/P-Luc mRNAs were pre-incubated with nuclear extracts of OL cells (total protein 1 to 4 µg) in a total 20 µl of binding mixture [10 mM HEPES (pH 7.6), 67 mM NaCl, 2 mM $MgCl_2$, 1 mM DTT, 1 mM EDTA, 5% glycerol, 10U RNasin] for 30 min at room temperature. For competition, a serial dilutions of decoy RNAs were pre-incubated with the extracts prior to the reaction. Binding mixtures were then subjected to the *in vitro* translation system using 50 µl of rabbit reticulocyte lysate (Promega), according to the manufacturer's recommendations. After incubation period of 2 h at 30°C, 10 µl of mixture was subjected to luciferase assay as described above.

RNA EMSA

The ^{32}P labeled-transcripts corresponding to the X/P and M/G UTRs were prepared with a mirVana miRNA Probe construction kit (Ambion), using PCR products or synthetic oligonucleotides as dsDNA templates. Transcription of the X/P and M/G UTRs was confirmed by their mobility in native PAGE. Unlabeled transcripts

were prepared with MEGAshortscript™ T7 Kit (Ambion). The cell extracts were obtained from exponentially growing OL cells. The cells were lysed with buffer A [20 mM HEPES (pH 7.6), 10 mM NaCl, 1.5 mM $MgCl_2$, 0.2 mM EDTA, 1 mM DTT, 0.1% NP-40, 20% glycerol and protease inhibitor cocktail] and then incubated on ice for 5 min. After collection of the cells, the lysate was incubated for a further 10 min. After centrifugation at 2,000 rpm for 5 min, the supernatant was collected as the cytoplasmic extract. The pellet was lysed with buffer B [20 mM HEPES (pH 7.6), 500 mM NaCl, 1.5 mM $MgCl_2$, 0.2 mM EDTA, 1 mM DTT, 0.1% NP-40, 20% glycerol and protease inhibitor cocktail], incubated on ice for 30 min and separated by centrifugation at 15,000 rpm for 15 min. The soluble nuclear fraction was diluted in binding buffer [10 mM HEPES (pH 7.6), 100 mM NaCl, 1.5 mM $MgCl_2$, 1 mM EDTA, 1 mM DTT, 0.1% NP-40, 10% glycerol]. About 1.0 pmol of ^{32}P-labeled gel-purified probes was incubated with the nuclear extracts (4 μg) in a total of 30 μl of binding mixture [10 mM HEPES (pH 7.6), 67 mM NaCl, 2 mM $MgCl_2$, 1 mM DTT, 1 mM EDTA, 5% glycerol, 20 μg tRNA, 10 U RNasin] for 20 min at room temperature. For competition, non-labeled probes were incubated with the nuclear extract for 20 min at room temperature prior to incubation with the labeled probes. For the assays using recombinant proteins, the probes were incubated with 5 pmol of GST-tagged DDX21 or nucleolin in a total of 20 μl of binding mixture [20 mM HEPES (pH7.5), 70 mM KCl, 2 mM $MgCl_2$, 2 mM DTT, 0.2 mg/ml BSA, 20 U RNasin] for 10 min at 30°C and for 10 min at room temperature. The reaction mixtures were applied to 4% native polyacrylamide gels (40:1 acrylamide-bisacrylamide) in TBE buffer. After electrophoresis, the gels were exposed to X-ray film overnight at −80°C.

RNA-affinity column purification of the 5′ UTR-binding proteins

Nuclear extracts of OL cells were prepared as described above. The nuclear extracts were passed through the RNA-negative coupled column and then loaded onto a consecutive RNA-positive column to remove nonspecific binding proteins. The extracts (total 2.5 mg of protein) were loaded on HiTrap Streptavidin HP column (1.0 ml bed volume; GE Healthcare) equilibrated with binding buffer three times (0.2 ml/min). The flow-through was incubated with 0.02 μmol of a 5′-biotinylated short (20 mer) RNA probe in binding buffer on ice for 30 min, and passed through a HiTrap column three times (0.2 ml/min). The column was washed with 30 ml binding buffer and then the proteins were eluted from the columns by the addition of binding buffer containing 600 mM NaCl. After dialysis with binding buffer, the sample was subjected to an X/P UTR- or M/G UTR-coupled column as a second step of RNA-affinity purification. After washing, the binding proteins were eluted from the column with the same as for the short RNA probe-coupled column.

LC-MS/MS

Samples eluted from the RNA affinity columns were separated on 10% SDS-PAGE and visualized by silver-staining (Wako). The protein bands of interest were excised, digested in-gel with trypsin, and analyzed by nanocapillary reversed-phase LC-MS/MS using a C18 column (φ 75 μm) on a nanoLC system (Ultimate, LC Packing) coupled to a quadrupole time-of-flight mass spectrometer (QTOF Ultima, Waters). Direct injection data-dependent acquisition was performed using one MS channel for every three MS/MS channels and dynamic exclusion for selected ions. Proteins were identified by database searching using Mascot Server (Matrix Science).

GST-pull down assay

For the protein pull-down assay, 200 pmol of recombinant His-DDX21 and approximately 100 pmol of truncated forms of GST-nucleolin were incubated with RIPA buffer for 1 h at 4°C. After the incubation, reaction mixtures were bound to glutathione-Sepharose 4B (Amersham Biosciences) in RIPA buffer overnight at 4°C. After washing with the same buffer three times, bound proteins were analyzed by immunoblotting with anti-DDX21 antibodies.

In vitro RNA folding assay

About 1.0 pmol of ^{32}P-labeled probes were heated at 85°C for 5 min, quickly cooled on ice and equilibrated at 23°C for 20 min prior to the reaction, unless manipulated further. These RNAs were incubated with 5 pmol of GST-tagged DDX21 and GST-tagged truncated nucleolin, Nuc(1234R) in total 15 μl of binding mixture [20mM HEPES (pH 7.5), 70 mM KCl, 3 mM ATP, 0.2 mg/ml BSA, 20 U RNasin] at 23°C for 20 min. After the incubation, the reaction was terminated by the addition of 5×loading buffer [20 mM HEPES (pH 7.5), 70 mM KCl, 50% glycerol, 0.5% SDS, 0.2 mg/ml proteinase K, 0.01% BPB, 0.01% XC], which also inactivated the enzyme. A part of the reaction mixtures was then applied to 12% native polyacrylamide gel (40:1 acrylamide-bisacrylamide) in TBE buffer. After electrophoresis, the gels were exposed to X-ray film overnight at −80°C.

In vitro RNA binding assay

The OL cells expressing Flag-tagged recombinant proteins were lysed with RIPA buffer including protease inhibitors and 40 μg/ml of RNase A, and IP were performed using anti-Flag M2 as described above. The precipitants were washed twice with washing buffer [20 mM Tris-HCl (pH 7.5), 70 mM NaCl, 70 mM KCl, 0.1% NP-40] and once with binding buffer [20 mM Tris-HCl (pH 7.5), 70 mM KCl, 0.1% NP-40] and subjected to *in vitro* binding assay. 10 pmol of ^{32}P-labeled X/P UTR probe was added to 20 μl of 50% suspension of the protein-loaded beads. After adjusting the total volume to 250 μl with binding buffer, the reaction mixture was incubated at 4°C for 10 min with gentle agitation. Unbound probe was removed by washing three times with 1 ml of binding buffer. The amount of bound radio-activity was measured by scintillation counting and the specificity was achieved by eliminating background activity obtained from the bead with the mock-transfected cell extract.

Supporting Information

Figure S1 The translation of X is suppressed at an early stage of BDV infection. BDV strain He80 was infected into C6 (rat glioma) or OL (human oligodendroglioma) cells. The subcellular localization of X and P was determined by immunofluorescence assay using anti-BDV P and X antibodies. The cells were analyzed when the infection rate was below 5% and reached 100% as early and persistent stages, respectively.
Found at: doi:10.1371/journal.ppat.1000654.s001 (0.54 MB PDF)

Figure S2 The translation of uORF influences translation of the X ORF. (A) Schematic representation of deletion mutants of the 5′ UTR of X/P expression plasmid. The nucleotide regions deleted from the wt plasmid are shown. The nucleotide region between 23 and 42 contains a short-stem loop structure shown in Figure S8. (B) OL cells were transfected with 0.8 μg of each plasmid and at 12 h after transfection cells were harvested and subjected to Western blotting using anti-BDV P and X antibodies. (C) Fold-activation of X expression in the cells transfected with mutant

plasmids was determined after quantitation of band intensities by ImageJ software.
Found at: doi:10.1371/journal.ppat.1000654.s002 (0.14 MB PDF)

Figure S3 Premature termination of uORF affects the expression of X. (A) Structure of uORF mutants. The nucleotide sequences substituted from the wt plasmid are indicated. These mutations do not induce structural modification of the 5′ UTR of X/P mRNA. (B) Expression of BDV P and X from the mutant uORF expression plasmids. OL cells cultured in 12 well culture dishes were transfected with 0.8 μg of wt and uORF mutant plasmids. Twelve h post-transfection, cells were lysed and subjected to western blot analysis using anti-BDV P and X antibodies. (C) Relative expression of X and P in uORF mutant plasmid-transfected OL cells. The band intensities shown in (B) were determined after quantitation by ImageJ software. The means plus S.D. of three independent experiments are shown. $^{**}P<0.01$, (Student's t test).
Found at: doi:10.1371/journal.ppat.1000654.s003 (0.17 MB PDF)

Figure S4 Additional 5′ or Kozak's stem-loop structures in the 5′ UTR inhibit translation initiation of X and P. (A and B) Expression of BDV P and X from the 5′ UTR mutant plasmids. Schematic structure of 5′ UTR mutants is shown. The 5′-stem and Kozak-stem were introduced upstream of the uAUG and by replacing with uORF coding sequence, respectively. OL cells cultured in 12-well culture dishes were transfected with 0.8 μg of each plasmid. Forty-eight h post-transfection, cells were lysed and subjected to western blot analysis using anti-BDV P and X antibodies. (C) Nucleotide sequences of artificial stem structures.
Found at: doi:10.1371/journal.ppat.1000654.s004 (0.17 MB PDF)

Figure S5 The predicted peptide of uORF does not influence translation of X ORF. (A) Structure of a uORF mutant. The nucleotide and amino acid sequences substituted from the wt plasmid are indicated by black squares. These mutations do not induce structural modification of the 5′ UTR of X/P mRNA. 1 (wt): wild-type uORF, 2: mutant uORF. (B) Expression of BDV P and X from the mutant uORF expression plasmid. OL cells cultured in 12-well culture dishes were transfected with 0.8 μg of wt and uORF mutant plasmids. Forty-eight h post-transfection, cells were lysed and subjected to western blot analysis using anti-BDV P and X antibodies. (C) Relative expression of X and P in uORF mutant plasmid-transfected OL cells. The band intensities shown in (B) were determined after quantitation by ImageJ software. The means plus S.D. of three independent experiments are shown.
Found at: doi:10.1371/journal.ppat.1000654.s005 (0.12 MB PDF)

Figure S6 BDV P does not affect the functions of eukaryotic initiation factors. (A) OL cells were transfected with Flag-tagged BDV N or P plasmid and, forty-eight h post-transfection, cells were lysed with RIPA or TNE buffer and then immunoprecipitated with Flag-M2 affinity gel. Immunoprecipitates were analyzed using the indicated antibodies. CE indicates cell extract. (B) Expression and phosphorylation of eIFs in BDV P-expressed cells. The cells expressing BDV N or P were analyzed by western blotting using the antibodies indicated. The phosphorylation of eIF2α was detected by phosphoserine 51-eIF2α antibody.
Found at: doi:10.1371/journal.ppat.1000654.s006 (0.26 MB PDF)

Figure S7 GST-pull down assay of recombinant nucleolin. (A) Schematic representation of truncation mutants of recombinant GST-fused nucleolin. (B) *In vitro* pull-down assay between His-tagged DDX21 and GST-fused recombinant nucleolins. 200 pmol of recombinant His-DDX21 and approximately 100 pmol of truncated GST-fused nucleolins were incubated with RIPA buffer for 1 h at 4°C. Proteins precipitated with glutathione-Sepharose beads were immunoblotted with anti-DDX21 antibody. Coomassie brilliant blue (CBB) staining of His-tagged DDX21 and GST-fused nucleolins at the top, which were bacterially expressed, purified, and used for *in vitro* binding.
Found at: doi:10.1371/journal.ppat.1000654.s007 (0.14 MB PDF)

Figure S8 The stability of the 5′ UTR controls translation of X ORF. (A) Schematic representation of a short stem-loop (SL) structure in the 5′ UTR. (B) Base-pair changing mutations were introduced within the SL region. The nucleotide substitutions are indicated by black squares. OL cells were transfected with 0.8 μg of wt and SL mutants, and at 48 h post-transfection, cells were subjected to western blotting using anti-BDV P mouse monoclonal and anti-BDV X rabbit polyclonal antibodies. Predicted free energies (kcal/mol) of SL structures are shown. (C) Relative expression of X and P was determined after quantitation of band intensities by ImageJ software. The mean plus S.D. of three independent experiments are shown.
Found at: doi:10.1371/journal.ppat.1000654.s008 (0.12 MB PDF)

Acknowledgments

We thank Dr. K. Saito of DNA-chip Development Center for Infectious Diseases (RIMD, Osaka University) for mass spectrometry analysis.

Author Contributions

Conceived and designed the experiments: YW KI KT. Performed the experiments: YW NO YH KT. Analyzed the data: YW KI KT. Contributed reagents/materials/analysis tools: YW NO YH. Wrote the paper: YW KT.

References

1. Kozak M (1989) The scanning model for translation: an update. J Cell Biol 108: 229–241.
2. Ryabova LA, Pooggin MM, Hohn T (2002) Viral strategies of translation initiation: ribosomal shunt and reinitiation. Prog Nucleic Acid Res Mol Biol 72: 1–39.
3. Kozak M (2002) Pushing the limits of the scanning mechanism for initiation of translation. Gene 299: 1–34.
4. Zheng ZM, Baker CC (2006) Papillomavirus genome structure, expression, and post-transcriptional regulation. Front Biosci 11: 2286–2302.
5. Flint SJ, Enquist LW, Krug RM, Racaniello VR, Skalka AM (2000) Translational control of viral gene expression. In: Flint SJ, ed. Principles of Virology: Molecular Biology, Pathogenesis, and Control. Washington, DC: ASM Press. pp 370–400.
6. Kozak M (2005) Regulation of translation via mRNA structure in prokaryotes and eukaryotes. Gene 361: 13–37.
7. Ryabova LA, Pooggin MM, Hohn T (2006) Translation reinitiation and leaky scanning in plant viruses. Virus Res 119: 52–62.
8. Latorre P, Kolakofsky D, Curran J (1998) Sendai virus Y proteins are initiated by a ribosomal shunt. Mol Cell Biol 18: 5021–5031.
9. Stacey SN, Jordan D, Williamson AJ, Brown M, Coote JH, et al. (2000) Leaky scanning is the predominant mechanism for translation of human papillomavirus type 16 E7 oncoprotein from E6/E7 bicistronic mRNA. J Virol 74: 7284–7297.
10. Racine T, Barry C, Roy K, Dawe SJ, Shmulevitz M, et al. (2007) Leaky scanning and scanning-independent ribosome migration on the tricistronic S1 mRNA of avian reovirus. J Biol Chem 282: 25613–25622.
11. Jackson RJ (2005) Alternative mechanisms of initiating translation of mammalian mRNAs. Biochem Soc Trans 33: 1231–1241.
12. Adhin MR, van Duin J (1990) Scanning model for translational reinitiation in eubacteria. J Mol Biol 213: 811–818.
13. Kozak M (1999) Initiation of translation in prokaryotes and eukaryotes. Gene 234: 187–208.
14. Churbanov A, Rogozin IB, Babenko VN, Ali H, Koonin EV (2005) Evolutionary conservation suggests a regulatory function of AUG triplets in 5′-UTRs of eukaryotic genes. Nucleic Acids Res 33: 5512–5520.
15. Iacono M, Mignone F, Pesole G (2005) uAUG and uORFs in human and rodent 5′untranslated mRNAs. Gene 349: 97–105.

16. Yamashita R, Suzuki Y, Nakai K, Sugano S (2003) Small open reading frames in 5′ untranslated regions of mRnas. C R Biol 326: 987–991.
17. Morris DR, Geballe AP (2000) Upstream open reading frames as regulators of mRNA translation. Mol Cell Biol 20: 8635–8642.
18. Sachs MS, Geballe AP (2006) Downstream control of upstream open reading frames. Genes Dev 20: 915–921.
19. Spevak CC, Park EH, Geballe AP, Pelletier J, Sachs MS (2006) her-2 upstream open reading frame effects on the use of downstream initiation codons. Biochem Biophys Res Commun 350: 834–841.
20. Hinnebusch AG (2005) Translational regulation of GCN4 and the general amino acid control of yeast. Annu Rev Microbiol 59: 407–450.
21. Tomonaga K, Kobayashi T, Ikuta K (2002) Molecular and cellular biology of Borna disease virus infection. Microbes Infect 4: 491–500.
22. de la Torre JC (2006) Reverse-genetic approaches to the study of Borna disease virus. Nat Rev Microbiol 4: 777–783.
23. Briese T, Schneemann A, Lewis AJ, Park YS, Kim S, et al. (1994) Genomic organization of Borna disease virus. Proc Natl Acad Sci U S A 91: 4362–4366.
24. Cubitt B, Oldstone C, de la Torre JC (1994) Sequence and genome organization of Borna disease virus. J Virol 68: 1382–1396.
25. Schneider U, Naegele M, Staeheli P, Schwemmle M (2003) Active borna disease virus polymerase complex requires a distinct nucleoprotein-to-phosphoprotein ratio but no viral X protein. J Virol 77: 11781–11789.
26. Perez M, Sanchez A, Cubitt B, Rosario D, de la Torre JC (2003) A reverse genetics system for Borna disease virus. J Gen Virol 84: 3099–3104.
27. Poenisch M, Unterstab G, Wolff T, Staeheli P, Schneider U (2004) The X protein of Borna disease virus regulates viral polymerase activity through interaction with the P protein. J Gen Virol 85: 1895–1898.
28. Poenisch M, Staeheli P, Schneider U (2008) Viral accessory protein X stimulates the assembly of functional Borna disease virus polymerase complexes. J Gen Virol 89: 1442–1445.
29. Kobayashi T, Watanabe M, Kamitani W, Tomonaga K, Ikuta K (2000) Translation initiation of a bicistronic mRNA of Borna disease virus: a 16-kDa phosphoprotein is initiated at an internal start codon. Virology 277: 296–305.
30. Kobayashi T, Zhang G, Lee BJ, Baba S, Yamashita M, et al. (2003) Modulation of Borna disease virus phosphoprotein nuclear localization by the viral protein X encoded in the overlapping open reading frame. J Virol 77: 8099–8107.
31. Poenisch M, Wille S, Staeheli P, Schneider U (2008) Polymerase read-through at the first transcription termination site contributes to regulation of borna disease virus gene expression. J Virol 82: 9537–9545.
32. Watanabe Y, Ibrahim MS, Hagiwara K, Okamoto M, Kamitani W, et al. (2007) Characterization of a Borna disease virus field isolate which shows efficient viral propagation and transmissibility. Microbes Infect 9: 417–427.
33. Yanai H, Kobayashi T, Hayashi Y, Watanabe Y, Ohtaki N, et al. (2006) A methionine-rich domain mediates CRM1-dependent nuclear export activity of Borna disease virus phosphoprotein. J Virol 80: 1121–1129.
34. Schwemmle M, Jehle C, Shoemaker T, Lipkin WI (1999) Characterization of the major nuclear localization signal of the Borna disease virus phosphoprotein. J Gen Virol 80: 97–100.
35. Bharti AK, Olson MO, Kufe DW, Rubin EH (1996) Identification of a nucleolin binding site in human topoisomerase I. J Biol Chem 271: 1993–1997.
36. Ginisty H, Sicard H, Roger B, Bouvet P (1999) Structure and functions of nucleolin. J Cell Sci 112(Pt 6): 761–772.
37. Jiang Y, Xu XS, Russell JE (2006) A nucleolin-binding 3′ untranslated region element stabilizes beta-globin mRNA in vivo. Mol Cell Biol 26: 2419–2429.
38. Fuller-Pace FV (2006) DExD/H box RNA helicases: multifunctional proteins with important roles in transcriptional regulation. Nucleic Acids Res 34: 4206–4215.
39. Schwemmle M, De B, Shi L, Banerjee A, Lipkin WI (1997) Borna disease virus P-protein is phosphorylated by protein kinase Cepsilon and casein kinase II. J Biol Chem 272: 21818–21823.
40. Volmer R, Monnet C, Gonzalez-Dunia D (2006) Borna disease virus blocks potentiation of presynaptic activity through inhibition of protein kinase C signaling. PLoS Pathog 2: e19. doi:10.1371/journal.ppat.0020019.
41. Mialon A, Thastrup J, Kallunki T, Mannermaa L, Westermarck J, et al. (2008) Identification of nucleolar effects in JNK-deficient cells. FEBS Lett 582: 3145–3151.
42. Yang C, Maiguel DA, Carrier F (2002) Identification of nucleolin and nucleophosmin as genotoxic stress-responsive RNA-binding proteins. Nucleic Acids Res 30: 2251–2260.
43. Schmid S, Mayer D, Schneider U, Schwemmle M (2007) Functional characterization of the major and minor phosphorylation sites of the P protein of Borna disease virus. J Virol 81: 5497–5507.
44. Calkhoven CF, Muller C, Leutz A (2000) Translational control of C/EBPalpha and C/EBPbeta isoform expression. Genes Dev 14: 1920–1932.
45. Horvath CM, Williams MA, Lamb RA (1990) Eukaryotic coupled translation of tandem cistrons: identification of the influenza B virus BM2 polypeptide. EMBO J 9: 2639–2647.
46. Ahmadian G, Randhawa JS, Easton AJ (2000) Expression of the ORF-2 protein of the human respiratory syncytial virus M2 gene is initiated by a ribosomal termination-dependent reinitiation mechanism. EMBO J 19: 2681–2689.
47. Meyers G (2003) Translation of the minor capsid protein of a calicivirus is initiated by a novel termination-dependent reinitiation mechanism. J Biol Chem 278: 34051–34060.
48. Luttermann C, Meyers G (2007) A bipartite sequence motif induces translation reinitiation in feline calicivirus RNA. J Biol Chem 282: 7056–7065.
49. Kojima KK, Matsumoto T, Fujiwara H (2005) Eukaryotic translational coupling in UAAUG stop-start codons for the bicistronic RNA translation of the non-long terminal repeat retrotransposon SART1. Mol Cell Biol 25: 7675–7686.
50. Powell ML, Brown TD, Brierley I (2008) Translational termination-re-initiation in viral systems. Biochem Soc Trans 36: 717–722.
51. Poyry TA, Kaminski A, Connell EJ, Fraser CS, Jackson RJ (2007) The mechanism of an exceptional case of reinitiation after translation of a long ORF reveals why such events do not generally occur in mammalian mRNA translation. Genes Dev 21: 3149–3162.
52. Henning D, So RB, Jin R, Lau LF, Valdez BC (2003) Silencing of RNA helicase II/Gualpha inhibits mammalian ribosomal RNA production. J Biol Chem 278: 52307–52314.
53. Holmstrom TH, Mialon A, Kallio M, Nymalm Y, Mannermaa L, et al. (2008) c-Jun supports ribosomal RNA processing and nucleolar localization of RNA helicase DDX21. J Biol Chem 283: 7046–7053.
54. Meijer HA, Thomas AA (2002) Control of eukaryotic protein synthesis by upstream open reading frames in the 5′-untranslated region of an mRNA. Biochem J 367: 1–11.
55. Geib T, Sauder C, Venturelli S, Hassler C, Staeheli P, et al. (2003) Selective virus resistance conferred by expression of Borna disease virus nucleocapsid components. J Virol 77: 4283–4290.
56. Schneider U (2005) Novel insights into the regulation of the viral polymerase complex of neurotropic Borna disease virus. Virus Res 111: 148–160.
57. Poenisch M, Wille S, Ackermann A, Staeheli P, Schneider U (2007) The X protein of borna disease virus serves essential functions in the viral multiplication cycle. J Virol 81: 7297–7299.
58. Nakamura Y, Takahashi H, Shoya Y, Nakaya T, Watanabe M, et al. (2000) Isolation of Borna disease virus from human brain tissue. J Virol 74: 4601–4611.

ELSEVIER

INSTITUT PASTEUR

Microbes and Infection 11 (2009) 394–402

www.elsevier.com/locate/micinf

Original article

Heat shock cognate protein 70 controls Borna disease virus replication via interaction with the viral non-structural protein X

Yohei Hayashi [a], Masayuki Horie [a], Takuji Daito [a], Tomoyuki Honda [a,b], Kazuyoshi Ikuta [a,c], Keizo Tomonaga [a,d,*]

[a] *Department of Virology, Research Institute for Microbial Diseases (BIKEN), Osaka University, 3-1 Yamadaoka, Suita, Osaka 565-0871, Japan*

[b] *Japan Society for the Promotion of Science (JSPS), Chiyoda-ku, Tokyo 102-8472, Japan*

[c] *Section of Viral Infections, Thailand–Japan Research Collaboration Center on Emerging and Re-emerging Infections (RCC-ERI), Nonthaburi 11000, Thailand*

[d] *PRESTO, Japan Science and Technology Agency (JST), Chiyoda-ku, Tokyo 102-0075, Japan*

Received 6 December 2008; accepted 17 January 2009
Available online 10 February 2009

Abstract

Borna disease virus (BDV) is a non-segmented, negative-sense RNA virus and has the property of persistently infecting the cell nucleus. BDV encodes a 10-kDa non-structural protein, X, which is a negative regulator of viral polymerase activity but is essential for virus propagation. Recently, we have demonstrated that interaction of X with the viral polymerase cofactor, phosphoprotein (P), facilitates translocation of P from the nucleus to the cytoplasm. However, the mechanism by which the intracellular localization of X is controlled remains unclear. In this report, we demonstrate that BDV X interacts with the 71 kDa molecular chaperon protein, Hsc70. Immunoprecipitation assays revealed that Hsc70 associates with the same region of X as P and, interestingly, that expression of P interferes competitively with the interaction between X and Hsc70. A heat shock experiment revealed that BDV X translocates into the nucleus, dependent upon the nuclear accumulation of Hsc70. Furthermore, we show that knockdown of Hsc70 by short interfering RNA decreases the nuclear localization of both X and P and markedly reduces the expression of viral genomic RNA in persistently infected cells. These data indicate that Hsc70 may be involved in viral replication by regulating the intracellular distribution of X.

Keywords: Borna disease virus; Protein X; Heat shock cognate protein 70; Nuclear localization; Virus replication

1. Introduction

Borna disease virus (BDV) belongs to the Bornaviridae family within the non-segmented negative-strand RNA viruses, Mononegavirales, which are characterized by highly neurotropic and noncytopathic infection of a wide variety of host species, including humans. Among the animal-derived mononegaviruses [1–4], BDV has several distinguishing features. One of the most striking characteristics is the cellular localization of its replication [5,6]. BDV RNA is transcribed and replicated in the nucleus, while other negative-strand RNA viruses replicate in the cytoplasm. Furthermore, unique among RNA viruses, BDV establishes a long-lasting persistent infection in both transformed and animal brain cell nuclei [5,6], suggesting that the virus uses mechanisms for RNA replication previously unknown in eukaryotic cells.

BDV encodes at least six different proteins. Of these, the nucleoprotein (N) and phosphoprotein (P) are major components of BDV ribonucleoproteins (RNPs) and are expressed abundantly in infected cells [7]. In addition to the other viral structural proteins, such as matrix and the envelope

* Corresponding author. Department of Virology, Research Institute for Microbial Diseases (BIKEN), Osaka University, 3-1 Yamadaoka, Suita, Osaka 565-0871, Japan. Tel.: +81 6 6879 8308; fax: +81 6 6879 8310.
E-mail address: tomonaga@biken.osaka-u.ac.jp (K. Tomonaga).

1286-4579/$ - see front matter © 2009 Elsevier Masson SAS. All rights reserved.
doi:10.1016/j.micinf.2009.01.006

glycoprotein, BDV produces a 10-kDa non-structural protein X, encoded by an open reading frame (ORF) which overlaps the P ORF by 215 nucleotides [7]. Previous studies using BDV minireplicon systems revealed that X strongly inhibits the polymerase activity of BDV, suggesting that it is a negative regulator of viral replication [8,9]. On the other hand, studies using reverse genetics have shown that a moderate level of X is required in infected cells for productive viral replication [10,11]. These observations indicate that X may control viral polymerase activity at the level needed to maintain a persistent infection in the nucleus. Although the precise mechanism by which X controls viral replication remains unclear, we reported previously that interaction of X with P promotes nuclear export of P, resulting in the cytoplasmic accumulation of both proteins [12,13]. P was retained in the cytoplasm of BDV-infected cells only when expression of X was detected in the same cell [12], suggesting that interaction between X and P reduces the level of P in the nucleus and thus prevents the formation of an active polymerase complex. Furthermore, Schwardt et al. demonstrated that BDV X may regulate viral polymerase activity via its direct incorporation into viral RNPs in the nucleus, because apparently X is present in BDV-specific nuclear dot structures where replication of BDV RNPs may occur [14]. All these observations suggest that the intracellular localization, as well as nuclear transport, of X may be important for the regulation of viral polymerase activity in infected cells. Although X is known to contain a non-canonical nuclear localization signal (NLS) within the N-terminal 20 amino acid domain and by itself localizes in the nucleus [15], it remains to be determined how a protein with a molecular mass of 10 kDa, which may be excluded by the nuclear pore, is maintained in the cell nucleus and then regulates viral polymerase activity.

In this study, we present data showing that BDV X interacts with the constitutive heat shock cognate 70 protein (Hsc70) in BDV-infected cells. We found that the N-terminal 16 amino acids of X are important for the interaction with Hsc70 and, interestingly, that their association is interfered with competitively by the expression of P. Heat shock stress of BDV-infected cells revealed that BDV X translocates rapidly into the nucleus in association with nuclear accumulation of Hsc70. Furthermore, analysis using short interfering RNA (siRNA) for Hsc70 demonstrated that knockdown of Hsc70 decreases the replication of the BDV genomic RNA, as well as the nuclear distribution of both X and P, in persistently infected cells. Our results suggested that Hsc70 may be involved in the nuclear localization of X and thereby regulate viral replication in the nucleus.

2. Materials and methods

2.1. Cell lines and virus

The OL cell line, derived from a human oligodendroglioma, was cultured in Dulbecco's modified Eagle's medium (DMEM)-high glucose (4.5%) supplemented with 5% fetal bovine serum (FBS) and 4 mM glutamine. HEK293T (293T; human embryonic kidney) cells were cultured in DMEM-low glucose (1.0%) supplemented with 5% FBS. BDV-infected OL cells, a cell line persistently infected with strain huP2br [16], were cultured using the same conditions as the parental cell line.

2.2. Plasmid construction

Constructions of expression vectors encoding Flag-tagged BDV P and X have been previously described [12]. To generate the eukaryotic expression plasmid encoding Flag-tagged N, BDV N cDNA was amplified by PCR and inserted into *Kpn* I and *Xho* I sites of pcDNA3 plasmid (Invitrogen). The hemagglutinin (HA)-tagged Hsc70 expression plasmid, pcHA-Hsc70, was constructed by the insertion of Hsc70 cDNA amplified from total RNA extracted from OL cells into *Kpn* I and *Xho* I sites of pcDNA-HA vector. The tandem tagged BDV X expression vector (pTAP-X) was generated as follows. The BDV cDNA corresponding to BDV X ORF was amplified with pgX plasmid [12] and digested with *Eco*R I and *Xho* I enzymes. The resultant fragment was inserted into the tandem affinity purification (TAP) assay vector (a kindly gift of Dr. Matsuura, Osaka University), which contain a HA-TEV (tobacco etch virus protease cleavage site)-Flag cassette sequence at the multiple cloning site of pcDNA3 vector.

2.3. TAP assay

Two days before transfection, 2.5×10^5 BDV-infected or uninfected OL cells were seeded in 60-mm culture dishes and transfected with pTAP-X by lipofectamine 2000 (Invitrogen). At 72 h post-transfection, the cells were harvested and lysed with TNE buffer (10 mM Tris–HCl, pH 8.0, 150 mM NaCl, 1 mM EDTA, 0.1 or 0.5% Nonidet P-40 [NP-40], and complete protease inhibitor) on ice for 60 min. After centrifugation, the soluble fraction was immunoprecipitated with anti-HA resin (Sigma–Aldrich) overnight at 4 °C. The resin was washed five times with TNE buffer and the tagged protein was released from the resin by digestion with AcTEV protease (Invitrogen) in 150 μL of TEV buffer containing 10 U protease for 3 h at 16 °C. TNE buffer was added to the supernatant from the centrifugation to increase the volume to 1 ml and the preparation was immunoprecipitated with anti-Flag M2 resin (Sigma–Aldrich) for 4 h at 4 °C. After washing five times with TNE buffer, the resin was incubated with 100 μl of TNE buffer containing 450 ng/μl of 3× Flag peptide (Sigma–Aldrich) for 3 h at 4 °C. The eluates were analyzed by SDS-PAGE and visualized by silver staining (Wako).

The protein bands of interest were excised, digested in-gel with trypsin, and analyzed by nanocapillary reversed-phase LC–MS/MS using a C18 column (φ 75 μm) on a nano LC system (Ultimate, LC Packing) coupled to a quadrupole time-of-flight mass spectrometer (QTOF Ultima, Waters). Direct injection data-dependent

acquisition was performed using one MS channel for every three MS/MS channels and dynamic exclusion for selected ions. Proteins were identified by database searching using Mascot Server (Matrix Science).

2.4. Indirect immunofluorescence assays

Cells were cultured on cover glass slides, fixed with 4% paraformaldehyde, and permeabilized with phosphate buffered saline (PBS) containing 0.4% Triton X-100 for 5 min at room temperature. The cells were then incubated with antibodies (anti-BDV antibodies, anti-Hsc70 antibody [Stressgen]) for 60 min in a humidified chamber at 37 °C. This was followed by incubation with appropriate Alexa Fluor-conjugated secondary antibodies (Invitrogen). A confocal laser-scanning microscope C1si (Nikon Inc.) was used for cell immunofluorescence imaging and data collection.

2.5. Western blot and immunoprecipitation analyses

For Western blotting, total cell lysates were subjected to SDS-PAGE and transferred onto polyvinylidene difluoride membranes (Millipore Corporation). We adjusted the amount of total proteins by applying the same volume of cell lysates to SDS-PAGE. Antibodies used in this study were as follows; rabbit anti-BDV P and anti-X [12], rat anti-Hsc70 (Stressgen), anti-Flag (Sigma-Aldrich) and anti-HA (Roche) antibodies.

For immunoprecipitation (IP) assay, 1.5×10^5 and 2×10^5 of OL and 293T cells, respectively, were seeded in 6 well plates before 48 h transfection and transfected with Flag- or HA-tagged plasmids by lipofectamine 2000 (Invitrogen). At 48 h post-transfection, cells were lysed with 1 ml of TNE buffer. After centrifugation at 15,000 rpm for 10 min, the supernatants were incubated with 40 μl of pre-equilibrated anti-Flag M2 agarose or anti-HA resin (Sigma–Aldrich) overnight at 4 °C with gentle rotation. After incubation, beads were collected by centrifugation at 6000 rpm for 40 s and washed three times with 1 ml of TNE buffer. The proteins immunoprecipitated with anti-Flag agarose or anti-HA resin were eluted and detected by Western blotting as described above.

2.6. Quantitative real-time RT-PCR (qRT-PCR)

Total RNA was extracted from BDV-infected cells and reverse transcribed with a Transcriptor First Strand cDNA Synthesis Kit (Roche) using a BDV-specific primer (5′-TGTTGCGCTAACAACAAACCAATCAC-3′) or an anchored oligo(dT) primer. Quantitative real-time RT-PCR assays were carried out using a gene-specific double fluorescent-labeled probe in the 7900HT Fast Real-Time PCR System (Applied Biosystems). The Taqman® probe was labeled with 6-carboxy fluorescein (FAM) as the 5′ fluorescent reporter and tetramethylrhodamine (TAMRA) as the 3′ quencher. The primers and probe used were as follows: BDV P-forward primer, 5′-ATGCATTGACCCAACCGGTA-3′; BDV P-reverse primer, 5′-ATCATTCGATAGCTGCTCCCTTC-3′; and BDV P-probe, 5′-FAM-AGAACCCCTCCATGATCTCA-GACCCAGA- TAMRA-3′. The amount of the first template was measured as follows. The threshold cycle (Ct) value was determined as the number of cycles at which a significant fluorescence increase was first detected. The threshold was automatically defined by the Sequence Detection System (ABI). The Ct-value was converted to a signal intensity by the method that assumes the difference of 1 cycle between samples produces a 2-fold difference.

2.7. siRNA expression

siRNAs for silencing of human Hsc70 were purchased from Qiagen. OL cells were transiently transfected using lipofectamine2000 (Invitrogen) with a final concentration of 100 nM for the siRNAs. After 48–72 h transfection, when protein levels of Hsc70 decreased to 10–20% of control cells, cells were subjected to experiments including heat stress assay.

3. Results and discussion

3.1. A non-structural BDV protein X interacts with Hsc70

To investigate the host factor(s) that interact with BDV X, a combination of TAP and LC-MS/MS analyses was conducted. We transfected pTAP-X into BDV-infected or uninfected OL cells, and then purified BDV X from the cell lysate using the TAP strategy described in Section 2. Proteins that interacted specifically with BDV X in the transfected cells were identified by SDS-PAGE followed by mass spectrometry analysis (Fig. 1A). In addition to BDV structural proteins (arrowheads), we identified a specific band around 70-kDa in both BDV-infected and uninfected cells and determined that this band corresponds to Hsc70. We verified their specificities by Western blotting (Fig. 1B).

To confirm the interaction between BDV X and Hsc70 in cells, we transfected Flag-tagged BDV N, P, or X protein into uninfected OL or 293T cells and performed immunoprecipitation assays using anti-Flag antibody. As shown in Fig. 1C, endogenous Hsc70 was clearly detected in the cells transfected only with the X-Flag plasmid in both cell lines, indicating that Hsc70 interacts specifically with BDV X, even in the absence of other viral components.

3.2. Interaction between Hsc70 and X is interfered by BDV P phosphoprotein

To understand the significance of the interaction between X and Hsc70, we first investigated the amino acid regions of X and Hsc70 required for the interaction. To map the interaction domain on X to Hsc70, we constructed a series of deletion mutants of the Flag-tagged X plasmid (Fig. 2A). We transfected the mutant plasmids into 293T cells and then performed immunoprecipitation assay using anti-Flag antibody. As shown in Fig. 2B, endogenous Hsc70 was detected by all the truncated X mutants, except for X-FlagΔ1, which lacks 16

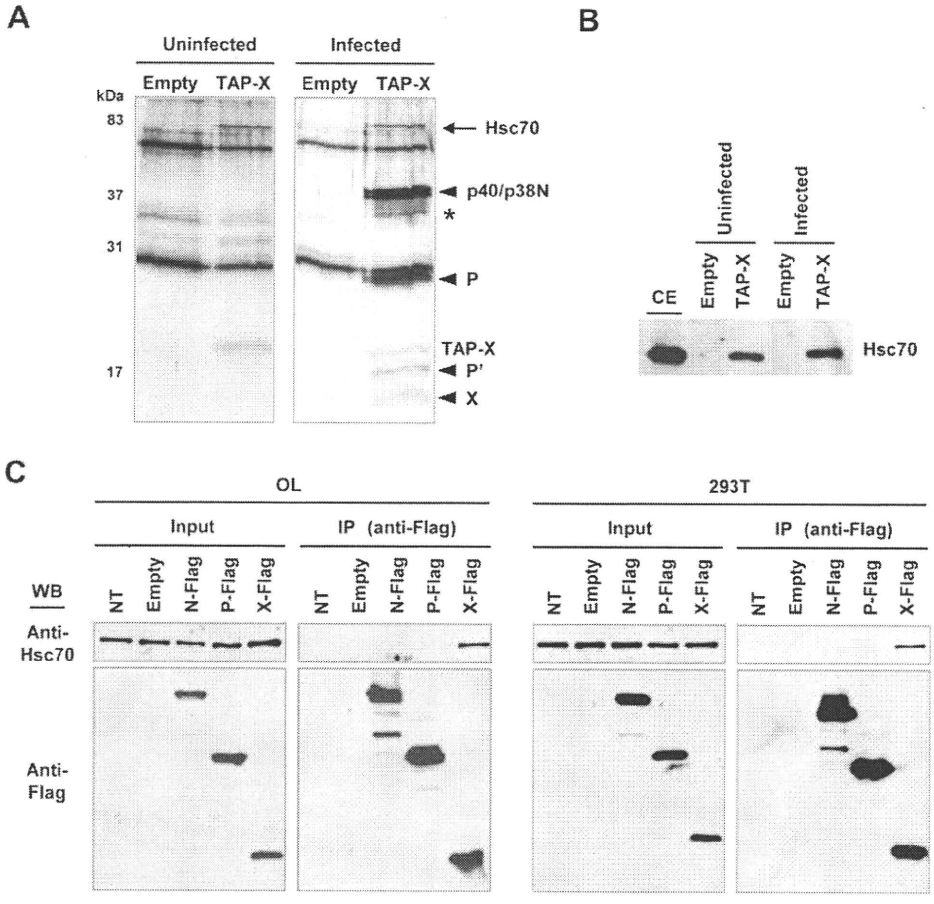

Fig. 1. BDV X interacts with Hsc70. (A and B) Tandem-affinity purification analysis of BDV X. Proteins that co-precipitated with TAP-X in uninfected and BDV-infected cells were separated by SDS-PAGE, visualized by silver staining (A), and identified by Western blotting (B). Arrowheads in panel (A) indicate BDV proteins. Asterisk indicates the degradation forms of BDV N. Empty; empty plasmid-transfected. (B) The proteins separated by PAGE in (A) were transferred onto polyvinylidene difluoride membranes and detected by Western blotting using anti-Hsc70 antibody. CE; cell extract from uninfected OL cells. (C) Immunoprecipitation analysis of Hsc70. Flag-tagged BDV proteins were transfected into OL and 293T cells and immunoprecipitated with anti-Flag antibody. Endogenous Hsc70 was detected by anti-Hsc70 antibody. NT; non-transfected.

amino acids at the N-terminus of X, indicating that the N-terminal region is essential for the interaction with Hsc70.

We next determined which Hsc70 domain interacts with BDV X. Because Hsc70 consists of three domains, ATPase, peptide-binding, and variable domains (Fig. 2C) [17], we introduced deletions corresponding to each domain of the protein (Fig. 2C). The truncated Hsc70 tagged with HA (HA-Hsc70) and Flag-X were co-transfected into 293T cells and subjected to immunoprecipitation using anti-HA antibody. As shown in Fig. 2D, the mutants which contain deletions in the peptide-binding domain (Hsc70Δ2 and Δ4) could not bind to X, whereas Hsc70 lacking the ATPase and variable domains (Hsc70Δ1 and Δ3) clearly precipitated X, indicating that the peptide-binding domain of Hsc70 is necessary for interaction with BDV X.

Previous studies demonstrated that a 16-amino acid stretch at the N-terminus of X contains the region that interacts with P [18]. This raises the possibility that P interferes competitively with the association of Hsc70 with X in BDV-infected cells. We therefore introduced X-Flag and HA-Hsc70 plasmids into OL cells with or without co-transfection of the P expression plasmid. As shown above, efficient interaction between X and Hsc70 was observed in the cells without transfection of P (Fig. 3A). On the other hand, co-expression of P clearly inhibited the immunoprecipitation from the cell lysates of Hsc70 and X by anti-Flag and anti-HA antibodies, respectively (Fig. 3A). The P mutant lacking the X-binding site, PΔM1 [19], failed to inhibit the interaction between X and Hsc70 (Fig. 3B), demonstrating competition between P and Hsc70 for interaction with X. Note that the immunoprecipitated level of X detected in the PΔM1-transfected cells appeared to be slightly reduced when compared with that in the empty-transfected cells. Considering the high phosphorylation property of P, it may be possible that the expression of PΔM1 perturbs the phosphorylation of proteins, including Hsc70 and X, in the cells, affecting the interaction between Hsc70 and X.

3.3. Hsc70 is involved in intracellular distribution of BDV X

To understand the role of the interaction between Hsc70 and X in the life cycle of BDV, we performed confocal

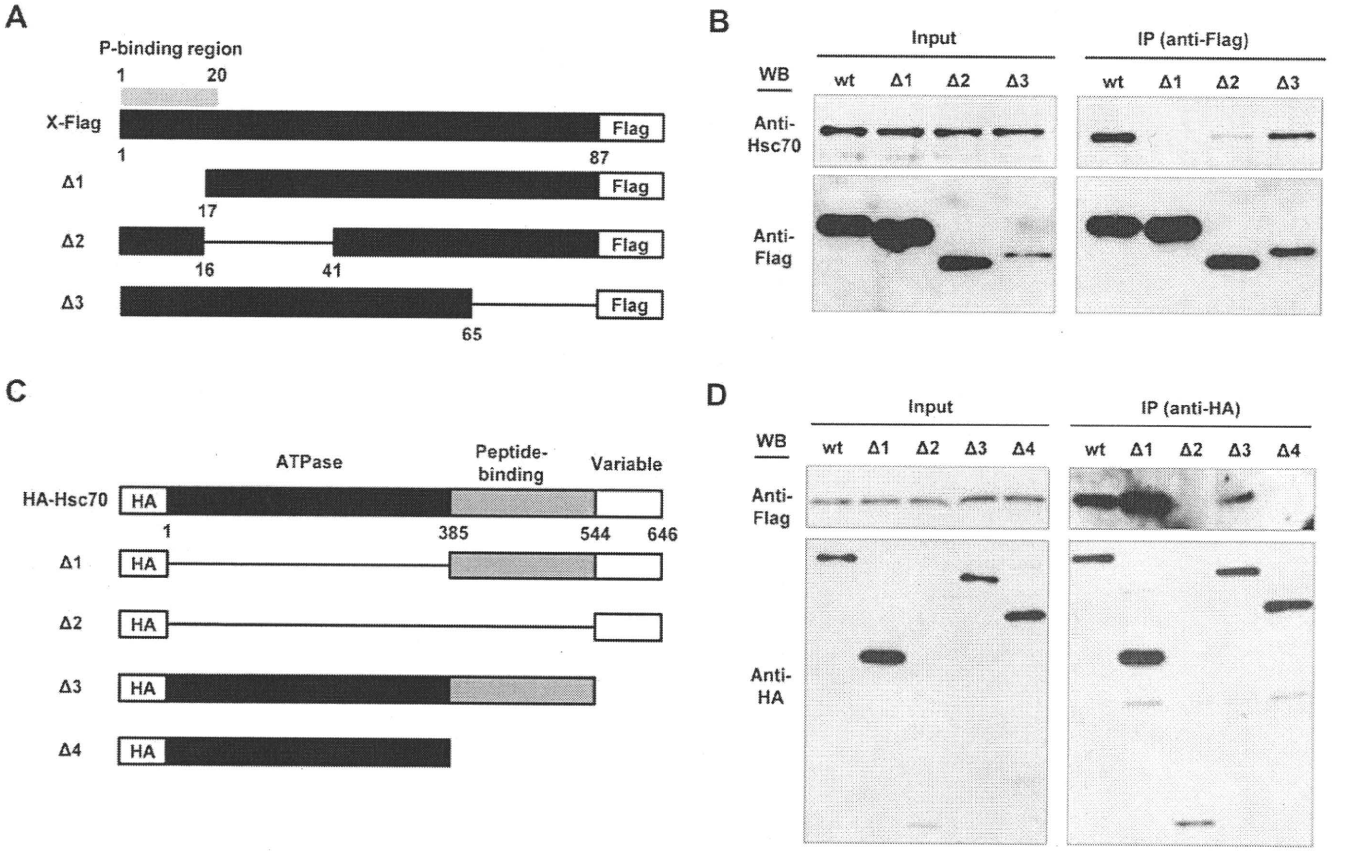

Fig. 2. Identification of interaction domains between BDV X and Hsc70. Identification of the regions of BDV X (A and B) and Hsc70 (C and D) necessary for their interaction. Schematic representations of Flag-X (A) and HA-Hsc70 (C) deletion mutants are shown. The numbers indicate amino acid positions in the proteins and known functional regions are indicated. The deletion plasmids were transfected into 293T (B) and OL (D) cells and immunoprecipitated by anti-Flag and anti-HA antibodies, respectively. Specific interaction was detected using anti-Hsc70 (B) or anti-Flag (D) antibody.

microscopic analysis of X and Hsc70 in BDV-infected OL cells. As reported previously [12,14,15], X localizes in both the cytoplasm and nucleus, along with the nuclear dot structures in BDV-infected cells (Fig. 4A). Hsc70 is also distributed diffusely in infected cells but is not incorporated into the BDV-specific nuclear dots (Fig. 4A). Hsc70 is known to facilitate the nuclear transport of wide variety of proteins, including viral proteins [20–24], as a molecular chaperone and to shuttle rapidly between the cytoplasm and nucleus [25,26]. Therefore, it is most likely that X, as a low molecular mass protein, uses Hsc70 to control its nuclear transport or intracellular localization in infected cells. To examine this, we exposed BDV persistently infected cells to heat stress to investigate whether inhibition of Hsc70 shuttling by the stress influences the distribution of X in infected cells. The cells were treated with a heat stress of 44 °C for 60 min with recovery at 37 °C [27], and intracellular localization of the proteins was observed at 3 h after the recovery. As reported in previous studies [25,26], heat stress inhibits the nuclear export of Hsc70, resulting in the accumulation of Hsc70 in the nucleus (Fig. 4A). Interestingly, the nuclear distribution of X also was observed in association with the accumulation of Hsc70 in the nucleus (Fig. 4A, B), suggesting that the intracellular localization of X may be dependent on the nuclear transport of Hsc70.

To examine further whether Hsc70 contributes to the intracellular distribution of X in BDV-infected cells, we transfected siRNA for Hsc70 into BDV-infected OL cells and monitored the intracellular localization of X and P. Interestingly, knockdown of Hsc70 appeared to decrease the distribution of both viral proteins in the nucleus, excluding the nuclear dot structures, at 48 h post-transfection (Figs. 4C, D and 5A). On the other hand, the intracellular distribution of BDV N was apparently unchanged by the knockdown of Hsc70 (Fig. 4E), suggesting that Hsc70 does not affect the nuclear distribution of viral RNPs. Considering that P may localize in the cytoplasm only when it forms a complex with X [12,13], the interaction between X and P seems to increase in the Hsc70-knockdown cells, leading to a reduction of nuclear localization of both the proteins.

3.4. Knockdown of Hsc70 decreases BDV replication in persistently infected cells

To determine whether Hsc70-knockdown impacts on BDV replication, we estimated the expression levels of both viral genomic RNA and mRNA by qRT-PCR in BDV-persistently infected OL cells transfected with Hsc70 siRNA (Fig. 5A). At 48 h after the siRNA treatment, the levels of genomic RNA,

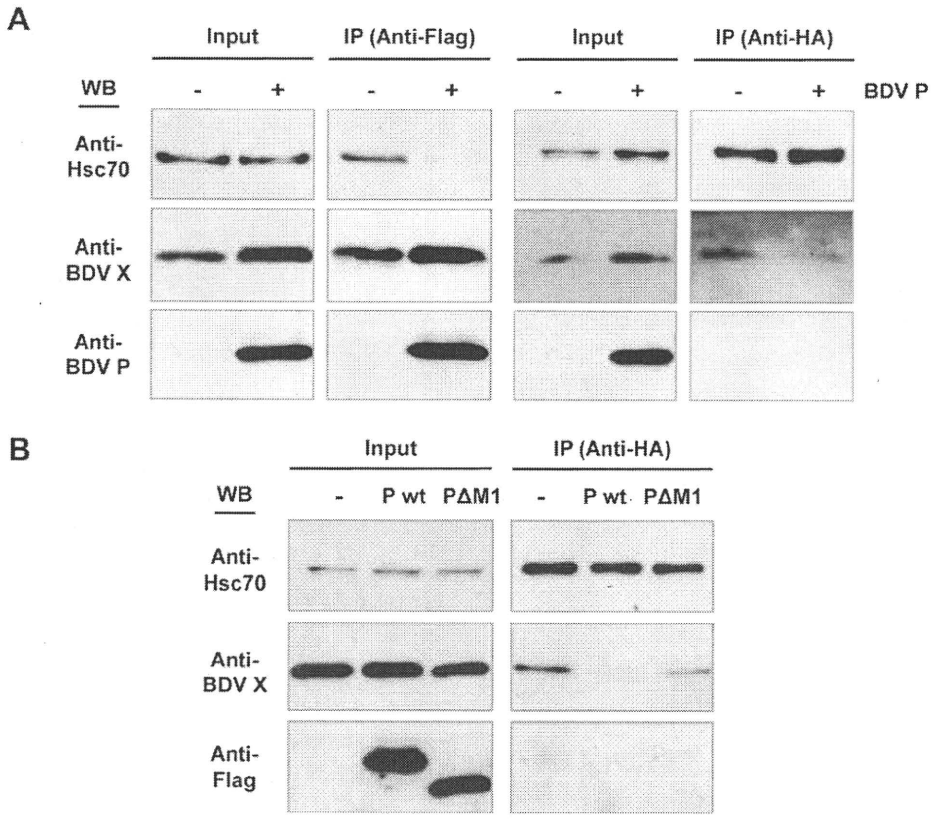

Fig. 3. BDV P interferes competitively with interaction between X and Hsc70. (A) Flag-tagged X and HA-tagged Hsc70 were cotransfected into OL cells with or without the BDV P expression plasmid. The lysates of the transfected cells were immunoprecipitated with anti-Flag or anti-HA antibody and the immunoprecipitates were analyzed using the antibodies indicated. (B) A BDV P mutant that lacks the region for binding to X failed to interfere with the interaction between X and Hsc70. The BDV mutant, PΔM1, was cotransfected with BDV X and Hsc70 expression plasmids, and the immunoprecipitations were performed as described above.

but not the mRNA, were reduced significantly in the infected cells (Fig. 5B). We observed the similar results in the expression of viral RNAs at 72 h post-transfection (data not shown). These results suggested that Hsc70 may mainly exert its effect on viral replication, rather than transcription, via regulation of the nuclear levels of the viral proteins.

3.5. Role of Hsc70 in BDV replication in the nucleus

Hsc70 is known to play multiple roles at different stages of a variety of viral life cycles. In influenza virus infection, Hsc70 is reported to interact directly with M1 protein and is required for the nuclear export of the viral RNP and production of virions [20]. Adenovirus also employs Hsc70 at various steps in its replication, including nuclear import and holding of the nucleocapsids [21]. Furthermore, the papillomavirus minor capsid protein L2 requires Hsc70 for nuclear translocation [22]. It has been reported that Hsc70 mediates the viral entry step of rotavirus [28], syncytium formation during human T-cell leukemia virus type I infection [29], and transcriptional regulation of herpes simplex virus [30]. From these observations, it is highly likely that, as a nuclear-dependent RNA virus, BDV also takes advantages of this host chaperon protein to control the replication activity in the nucleus.

In this study, we demonstrate that Hsc70 interacts specifically with a BDV non-structural protein, X (Fig. 1) and that their interaction is competitively interfered by P (Fig. 3). Hsc70-specific siRNA decreases the nuclear levels of X and P (Fig. 4) and causes a reduction in virus replication (Fig. 5). Previous reports revealed that BDV polymerase activity is tightly regulated by the N-to-P stoichiometry in the nucleus and that X may play a key role in the regulation of viral replication [8–11]. Although details of the mechanism by which X controls viral replication have not been elucidated yet, recent studies suggest possible mechanisms by which X influences the viral polymerase activity by promoting the translocation of P from the nucleus to the cytoplasm or by direct interaction with viral RNPs in the nucleus [12–14]. In either way, the nuclear level of X must be a critical determinant of the polymerase activity in the nucleus. Therefore, a mechanism for controlling the nuclear distribution of X may be present in infected cells. The present data show that the intracellular distribution may be controlled by the interaction with Hsc70. The dominant interaction of X with Hsc70 in the nucleus results in a reduction of the binding between X and P, leading to an increase in the nuclear level of P. This, in turn, could modify the polymerase activity in the nucleus. Although we could not determine whether P or Hsc70 dominantly interacts with X in infected cells, it is

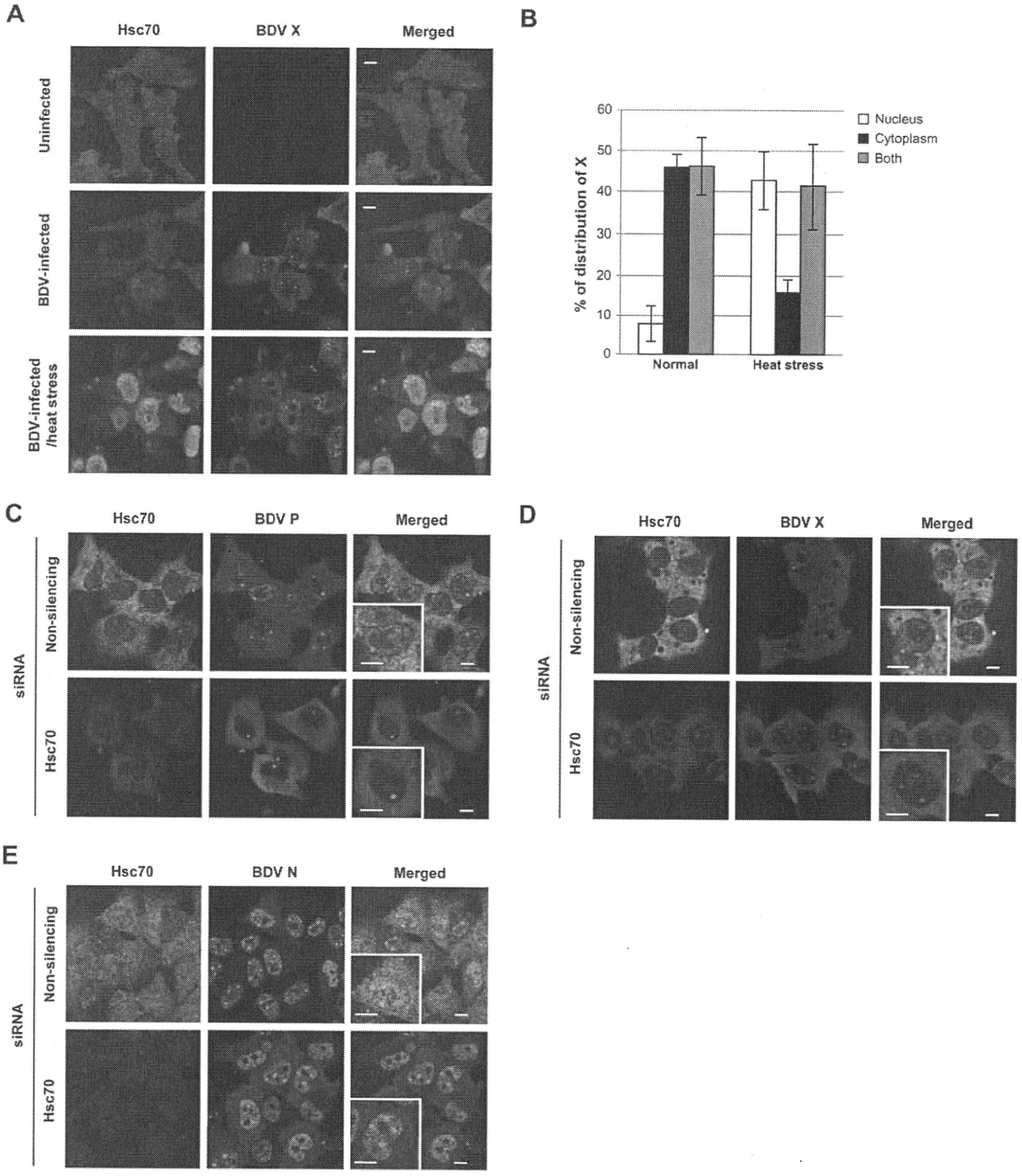

Fig. 4. Hsc70 is involved in intracellular localization of BDV X. (A) BDV persistently infected and uninfected OL cells were exposed to heat shock at 44 °C and allowed to recover at 37 °C for 3 h. Cells were fixed before and after the recovery time, and the intracellular distributions of BDV X and Hsc70 were visualized by indirect immunofluorescence assay using anti-X and anti-Hsc70 antibodies. The nuclei are visualized by 4′,6′-diamidino-2-phenylindole (DAPI) in merged panels. Bar, 10 μm. (B) BDV X translocates to the nucleus by heat stress. After 3 h of recovery, the subcellular localization of X was visualized by the immunofluorescence assay, and the percentage of cells showing each type of X distribution in the cells was determined. (C–E) Alteration of intracellular localization of BDV P (C), X (D) and N (E) in Hsc70 siRNA-treated BDV infected OL cells. Forty-eight hours after transfection of Hsc70 siRNA, the intracellular distributions of Hsc70 and BDV proteins were detected by anti-Hsc70 and either anti-P (C), anti-X (D) or anti-N (E) antibodies. Insets contain 1.7× magnifications of a cell nucleus. Bar, 10 μm.

conceivable that the dominant association among Hsc70, X, and P may be altered depending on the distribution of the proteins within the cells. Further studies regarding the functional interaction among the proteins will provide new insights into the regulation of BDV infection in the nucleus.

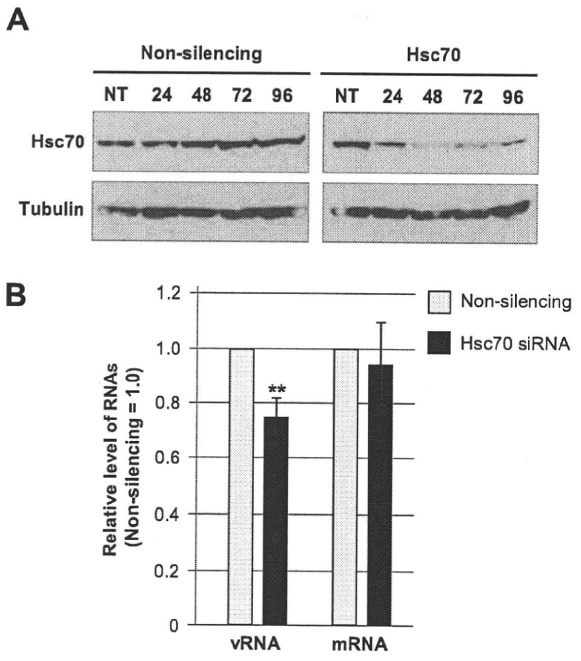

Fig. 5. Hsc70 knockdown reduces the level of BDV genomic RNA. BDV persistently infected cells were treated with Hsc70 specific siRNA and, 48 h post-transfection, expression levels of BDV genomic RNA and mRNA were quantified by qRT-PCR as described in Section 2. (A) The expression dynamics of Hsc70 in the siRNA-treated cells was monitored by Western blot analysis. (B) The relative expressions of BDV genomic RNA and mRNA are shown. Values were expressed as mean plus S.D. $^{**}P < 0.01$ (Student's t test). At least four-independent, triplicate experiments were performed.

Acknowledgments

We thank K. Saito of DNA-chip Development Center for Infectious Diseases (RIMD, Osaka University) for mass spectrometry analysis. This work was supported by Ministry of Education, Culture, Sports, Science and Technology (MEXT) Grants-in-aid for Scientific Research on Priority Areas (Infection and Host Responses; Matrix of Infection Phenomena) and PRESTO from Japan Science and Technology Agency (JST).

References

[1] K. Ikuta, K. Hagiwara, H. Taniyama, N. Nowotny, Epidemiology and infection of natural animal hosts, in: K.M. Carbone (Ed.), Borna disease virus and its role in neurobehavioral disease, ASM Press, Washington, DC, 2002, pp. 87–123.

[2] H. Ludwig, L. Bode, Borna disease virus: new aspects on infection, disease, diagnosis and epidemiology, Rev. Sci. Technol. 19 (2000) 259–288.

[3] K.M. Carbone, Borna disease virus and human disease, Clin. Microbiol. Rev. 14 (2001) 513–527.

[4] L. Bode, H. Ludwig, Borna disease virus infection, a human mental-health risk, Clin. Microbiol. Rev. 16 (2003) 534–545.

[5] K. Tomonaga, T. Kobayashi, K. Ikuta, Molecular and cellular biology of Borna disease virus infection, Microbes Infect. 4 (2002) 491–500.

[6] J.C. de la Torre, Reverse-genetic approaches to the study of Borna disease virus, Nat. Rev. Microbiol. 4 (2006) 777–783.

[7] U. Schneider, Novel insights into the regulation of the viral polymerase complex of neurotropic Borna disease virus, Virus Res. 111 (2005) 148–160.

[8] U. Schneider, M. Naegele, P. Staeheli, M. Schwemmle, Active Borna disease virus polymerase complex requires a distinct nucleoprotein-to-phosphoprotein ratio but no viral X protein, J. Virol. 77 (2003) 11781–11789.

[9] M. Perez, A. Sanchez, B. Cubitt, D. Rosario, J.C. de la Torre, A reverse genetics system for Borna disease virus, J. Gen. Virol. 84 (2003) 3099–3104.

[10] M. Poenisch, S. Wille, A. Ackermann, P. Staeheli, U. Schneider, The X protein of Borna disease virus serves essential functions in the viral multiplication cycle, J. Virol. 81 (2007) 7297–7299.

[11] M. Poenisch, P. Staeheli, U. Schneider, Viral accessory protein X stimulates the assembly of functional Borna disease virus polymerase complexes, J. Gen. Virol. 89 (2008) 1442–1445.

[12] T. Kobayashi, G. Zhang, B.J. Lee, S. Baba, M. Yamashita, W. Kamitani, H. Yanai, K. Tomonaga, K. Ikuta, Modulation of Borna disease virus phosphoprotein nuclear localization by the viral protein X encoded in the overlapping open reading frame, J. Virol. 77 (2003) 8099–8107.

[13] H. Yanai, T. Kobayashi, Y. Hayashi, Y. Watanabe, N. Ohtaki, G. Zhang, J.C. de la Torre, K. Ikuta, K. Tomonaga, A methionine-rich domain mediates CRM1-dependent nuclear export activity of Borna disease virus phosphoprotein, J. Virol. 80 (2006) 1121–1129.

[14] M. Schwardt, D. Mayer, R. Frank, U. Schneider, M. Eickmann, O. Planz, T. Wolff, M. Schwemmle, The negative regulator of Borna disease virus polymerase is a non-structural protein, J. Gen. Virol. 86 (2005) 3163–3169.

[15] T. Wolff, G. Unterstab, G. Heins, J.A. Richt, M. Kann, Characterization of an unusual importin alpha binding motif in the Borna disease virus p10 protein that directs nuclear import, J. Biol. Chem. 277 (2002) 12151–12157.

[16] Y. Nakamura, H. Takahashi, Y. Shoya, T. Nakaya, M. Watanabe, K. Tomonaga, K. Iwahashi, K. Ameno, N. Momiyama, H. Taniyama, T. Sata, T. Kurata, J.C. de la Torre, K. Ikuta, Isolation of Borna disease virus from human brain tissue, J. Virol. 74 (2000) 4601–4611.

[17] P. Lopez-Buesa, C. Pfund, E.A. Craig, The biochemical properties of the ATPase activity of a 70-kDa heat shock protein (Hsp70) are governed by the C-terminal domains, Proc. Natl. Acad. Sci. U.S.A. 95 (1998) 15253–15258.

[18] T. Wolff, R. Pfleger, T. Wehner, J. Reinhardt, J.A. Richt, A short leucine-rich sequence in the Borna disease virus p10 protein mediates association with the viral phospho- and nucleoproteins, J. Gen. Virol. 81 (2000) 939–947.

[19] G. Zhang, T. Kobayashi, W. Kamitani, S. Komoto, M. Yamashita, S. Baba, H. Yanai, K. Ikuta, K. Tomonaga, Borna disease virus phosphoprotein represses p53-mediated transcriptional activity by interference with HMGB1, J. Virol. 77 (2003) 12243–12251.

[20] K. Watanabe, T. Fuse, I. Asano, F. Tsukahara, Y. Maru, K. Nagata, K. Kitazato, N. Kobayashi, Identification of Hsc70 as an influenza virus matrix protein (M1) binding factor involved in the virus life cycle, FEBS Lett. 580 (2006) 5785–5790.

[21] A.C. Saphire, T. Guan, E.C. Schirmer, G.R. Nemerow, L. Gerace, Nuclear import of adenovirus DNA in vitro involves the nuclear protein import pathway and hsc70, J. Biol. Chem. 275 (2000) 4298–4304.

[22] L. Florin, K.A. Becker, C. Sapp, C. Lambert, H. Sirma, M. Muller, R.E. Streeck, M. Sapp, Nuclear translocation of papillomavirus minor capsid protein L2 requires Hsc70, J. Virol. 78 (2004) 5546–5553.

[23] S. Kose, M. Furuta, M. Koike, Y. Yoneda, N. Imamoto, The 70-kD heat shock cognate protein (hsc70) facilitates the nuclear export of the import receptors, J. Cell Biol. 171 (2005) 19–25.

[24] F. Tsukahara, Y. Maru, Identification of novel nuclear export and nuclear localization-related signals in human heat shock cognate protein 70, J. Biol. Chem. 279 (2004) 8867–8872.

[25] A. Chu, N. Matusiewicz, U. Stochaj, Heat-induced nuclear accumulation of hsc70s is regulated by phosphorylation and inhibited in confluent cells, FASEB J. 15 (2001) 1478–1480.

[26] M. Kodiha, A. Chu, O. Lazrak, U. Stochaj, Stress inhibits nucleocytoplasmic shuttling of heat shock protein hsc70, Am. J. Physiol. Cell Physiol. 289 (2005) C1034–1041.

[27] M. Yamashita, W. Kamitani, H. Yanai, N. Ohtaki, Y. Watanabe, B.J. Lee, S. Tsuji, K. Ikuta, K. Tomonaga, Persistent Borna disease virus infection confers instability of HSP70 mRNA in glial cells during heat stress, J. Virol. 79 (2005) 2033–2041.

[28] S. Lopez, C.F. Arias, Multistep entry of rotavirus into cells: a Versaillesque dance, Trends Microbiol. 12 (2004) 271–278.

[29] Y. Sagara, C. Ishida, Y. Inoue, H. Shiraki, Y. Maeda, 71-kilodalton heat shock cognate protein acts as a cellular receptor for syncytium formation induced by human T-cell lymphotropic virus type 1, J. Virol. 72 (1998) 535–541.

[30] L. Li, L.A. Johnson, J.Q. Dai-Ju, R.M. Sandri-Goldin, Hsc70 focus formation at the periphery of HSV-1 transcription sites requires ICP27, PLoS ONE 3 (2008) e1491.

Official Journal of the Asian Pacific Society of Respirology
Respirology

ORIGINAL ARTICLE

Carbocisteine inhibits oxidant-induced apoptosis in cultured human airway epithelial cells

MOTOKI YOSHIDA,[1] KATSUTOSHI NAKAYAMA,[2] HIROYASU YASUDA,[3] HIROSHI KUBO,[4] KAZUYOSHI KUWANO,[2] HIROYUKI ARAI[1] AND MUTSUO YAMAYA[4]

Departments of [1]Geriatrics and Gerontology and [4]Advanced Preventive Medicine for Infectious Disease, Tohoku University School of Medicine, Sendai, [2]Division of Respiratory Diseases, Department of Internal Medicine, Jikei University School of Medicine, Tokyo, and [3]Department of Translational Clinical Oncology, Kyoto University Graduate School of Medicine, Kyoto, Japan

ABSTRACT

Background and objective: **Increased oxidant levels have been associated with exacerbations of COPD, and L-carbocisteine, a mucolytic agent, reduces the frequency of exacerbations. The mechanisms underlying the inhibitory effects of L-carbocisteine on oxidant-induced COPD exacerbations were examined in an *in vitro* study of human airway epithelial cells.**

Methods: **In order to examine the antioxidant effects of L-carbocisteine, human tracheal epithelial cells were treated with L-carbocisteine and exposed to hydrogen peroxide (H_2O_2). Cell apoptosis was assessed using a cell death detection ELISA, and the pathways leading to cell apoptosis were examined by measurement of caspase-3 and caspase-9 by western blot analysis with fluorescent detection.**

Results: **The proportion of apoptotic cells in human tracheal epithelium was increased in a concentration- and time-dependent manner, following exposure to H_2O_2. Treatment with L-carbocisteine reduced the proportion of apoptotic cells. In contrast, H_2O_2 did not increase the concentration of LDH in supernatants of epithelial cells. Exposure to H_2O_2 activated caspase-3 and caspase-9, and L-carbocisteine inhibited the H_2O_2-induced activation of these caspases. L-carbocisteine activated Akt phosphorylation, which modulates caspase activation, and the inhibitors of Akt, LY294002 and wortmannin, significantly reversed the inhibitory effects of L-carbocisteine on H_2O_2-induced cell apoptosis.**

Conclusions: **These findings suggest that in human airway epithelium, L-carbocisteine may inhibit cell damage induced by H_2O_2 through the activation of Akt phosphorylation. L-carbocisteine may have antioxidant effects, as well as mucolytic activity, in inflamed airways.**

SUMMARY AT A GLANCE

The antioxidant effects of L-carbocisteine, a mucolytic agent, have not been studied. The inhibitory effects of L-carbocisteine on oxidant-induced cell damage were examined in human airway epithelial cells. Treatment with L-carbocisteine reduced the proportion of apoptotic cells after exposure to hydrogen peroxide. L-carbocisteine may also have antioxidant effects in the airways.

Key words: antioxidant, apoptosis, chronic obstructive pulmonary disease, emphysema, infection and inflammation, mucolytic.

INTRODUCTION

The mucolytic agent, N-acetylcysteine (NAC), has various physiological functions, including antioxidant effects,[1] anti-inflammatory effects[2] and modulation of mucin expression induced by LPS.[3] NAC has been suggested to have clinical benefits in the treatment of IPF, chronic bronchitis and COPD.[4–6] Likewise, mucolytic agents other than NAC, such as ambroxol and L-carbocisteine, also have various physiological functions, including improvement of airway mucociliary transport, modulation of neutrophil activation, inhibition of pro-inflammatory cytokine and mucin 5AC protein production in the airways, as well as anti-viral effects.[7–11] Furthermore, these mucolytic agents have been reported to reduce the frequency of COPD exacerbations.[12]

Exacerbations of COPD are caused by bacterial and viral infections of the airways,[13] and by exposure to oxidants.[14] On the other hand, increased levels of oxidants and substrates, including hydrogen peroxide

Correspondence: Motoki Yoshida, Department of Geriatrics and Gerontology, Tohoku University School of Medicine, Seiryo-machi, Aoba-ku, Sendai, 980-8574 Japan. Email: mtkyoshida@idac.tohoku.ac.jp

Conflict of interest statement: Matsuo Yamaya and Hiroshi Kubo have received funding from Kyorin Pharmaceutical Co., Ltd. for research carried out as part of this study.

Received 6 August 2008; invited to revise 31 October 2008, 2 March 2009; revised 27 January 2009, 17 March 2009; accepted 18 March 2009 (Associate Editor: Martin Kolb).

(H_2O_2), nitric oxide, ethane, carbon monoxide and isopentane, have been demonstrated in exhaled air or breath condensate, suggesting a role for oxidants in the pathogenesis of COPD.[15–17]

L-carbocisteine, a mucolytic agent, reduces the frequencies of common colds and exacerbations in patients with COPD,[18] and inhibits the production of pro-inflammatory cytokines and intracellular adhesion molecule-1,[9] which is a major rhinovirus receptor and activator of inflammatory cells in the airways. Therefore, L-carbocisteine may modulate airway inflammation induced by oxidants, as well as viral and bacterial infections that lead to COPD exacerbations. Furthermore, L-carbocisteine inhibits rhinovirus infection of airway epithelial cells,[9] which is a major cause of COPD exacerbations. However, except for the antioxidant effects of NAC[1] and carbocysteine lysine salt monohydrate,[19] the inhibitory effects of L-carbocisteine on oxidant-induced cell damage have not been studied.

In the present study, the antioxidant effects of L-carbocisteine and its effects on H_2O_2-induced apoptosis of human tracheal epithelial cells were examined. In addition, the mechanisms of the antioxidant effects of L-carbocisteine in airway epithelial cells were studied.

METHODS

Human tracheal epithelial cell culture

Reagents for cell culture were obtained as follows: Dulbecco's modified Eagle's medium, Ham's F-12 medium, PBS and foetal calf serum (FCS) were from GIBCO-BRL Life Technologies, Palo Alto, CA, USA; Ultroser G (USG) was from BioSepra, Cergy-Saint-Christophe, France, and trypsin-EDTA was from Sigma Chemical Co., St. Louis, MO, USA.

Tracheas were obtained immediately after death from 32 patients (mean age 75 ± 4 years; 15 female, 17 male), who did not have bronchial asthma or COPD, except for one patient with COPD. The causes of death included malignant tumours other than lung cancer ($n = 15$), congestive heart failure ($n = 8$), acute myocardial infarction ($n = 3$), cerebral bleeding ($n = 2$), renal failure ($n = 2$), rupture of an aortic aneurysm ($n = 1$) and cerebral infarction ($n = 1$). Ten patients were ex-smokers, and 22 had been non-smokers. The study was approved by the Tohoku University Ethics Committee.

Isolation and culture of human tracheal surface epithelial cells were performed as described previously.[20,21] The cells were suspended in 5 mL of Dulbecco's modified Eagle's medium–Ham's F-12 (DF-12) medium (50:50, vol/vol) containing 2% USG and antibiotics, plated at 1×10^6 viable cells per 5 mL in T25 tissue culture flasks (Costar Corning, Cambridge, MA, USA) coated with human placental collagen, and cultured at 37°C in 5% CO_2–95% air. When they had reached confluence (5–7 days), cells were collected by trypsinization (0.05% trypsin, 0.02% EDTA), replaced in 24-well dishes (2×10^5 viable cells/mL) in DF-12 medium containing 2% USG and antibiotics, and cultured at 37°C in 5% CO_2–95% air.

Assessment of DNA fragmentation by cell death detection ELISA

Cell viability was assessed using a cell death detection ELISA (Roche Diagnostics, Basel, Switzerland) according to the manufacturer's instructions.[22] Human tracheal epithelial cells, cultured in 200 μL of DF-12 medium containing 2% USG and antibiotics in 24-well dishes were pretreated with L-carbocisteine (10 μmol/L) or vehicle (0.1% double-distilled water; ddH_2O) for 72 h. Cells were then treated with H_2O_2 (400 or 800 μmol/L) or vehicle (0.1% ddH_2O) for 12 or 24 h. In preliminary experiments 400 μmol/L H_2O_2 decreased cell viability at 12 h, and the effects of 400 or 800 μmol/L H_2O_2 were therefore compared. In some experiments, cells were pretreated with L-carbocisteine (10 μmol/L) for 72 h, then treated with the Akt inhibitors, LY294002 (50 μmol/L, 30 min) or wortmannin (50 nmol/L, 30 min) (Wako Pure Chemical Co., Osaka, Japan), or vehicle (0.1% ddH_2O) before exposure to H_2O_2 (800 μmol/L). Culture supernatants were collected by centrifugation (200 × g, 10 min) and stored at 4°C before assay. Supernatant samples were incubated with biotinylated anti-histone antibody and anti-DNA antibody bound to peroxidase in microtitre plates coated with streptavidin, for 2 h at room temperature with shaking (300 rpm). The supernatants were then aspirated and the wells were rinsed three times with incubation buffer. To determine the amount of retained peroxidase, 2,2′-azino-di (3-ethylbenzthiazolin-sulphonate) and H_2O_2 were added as substrates, and the complex was measured in a spectrophotometer (SpectraMax 340PC384, Molecular Devices, Sunnyvale, CA, USA) at 405 nm.

Western blot analysis

Assessment of caspase-3, caspase-9, Akt and phospho-Akt was performed by western blot analysis.[23] Human tracheal epithelial cells at 80% confluence were cultured with or without L-carbocisteine (10 μmol/L) for 72 h and then treated with H_2O_2 (800 μmol/L) for 8 h.[24] The cells were suspended in modified radioimmunoprecipitation assay lysis buffer with 1× protease inhibitor (Roche, Mannheim, Germany). Cell extracts were centrifuged and supernatant was mixed with 2× sodium dodecyl sulphate-polyacrylamide gel electrophoresis sample buffer and boiled for 5 min. The sample was subjected to 15% sodium dodecyl sulphate-polyacrylamide gel electrophoresis and transferred to polyvinylidene difluoride membranes (Millipore, Billerica, MA, USA). Membranes were blotted with antibodies to caspase-3, caspase-9 and Akt or phospho-Akt (Cell Signaling Technology, Beverly, MA, USA). In addition, to ensure equal protein loading, the membranes were blotted with an antibody to β-actin (Sigma). The membranes

were developed using an enhanced chemiluminescence Advance Western Blotting Detection Kit (Amersham Biosciences, Pittsburgh, PA, USA) and a Lumino Image Analyzer (LAS-1000, Fuji Film, Tokyo, Japan) according to the manufacturer's instructions. Quantification of western blot bands was accomplished using National Institutes of Health Image v1.62 software. The average values from replicate cultures of the same trachea ($n = 3$) were used for analysis of the intensities of the western blot bands.

Assessment of caspase-3 activity

Caspase-3 activity was assessed using the Apo-ONE Homogeneous Caspase-3/7 Assay (Promega, Madison, WI, USA) according to the manufacturer's instructions. Human tracheal epithelial cells (4×10^4/100 μL), cultured in 96-well culture dishes, were pretreated with L-carbocisteine (1 or 10 μmol/L) for 72 h. Cells were then treated with H_2O_2 (400 or 800 μmol/L) for 8 h at room temperature, and mixed with the assay reagent (100 μL). The assay reagent was prepared by mixing the profluorescent substrate, bis-(N-CBZ-L-aspartyl-L-glutamyl-L-valyl-aspartic acid amide) rhodamine 110 (Z-DEVD-rhodamine 110) with buffer. This reagent lyses and permeabilizes cells, enabling optimal measurement of caspase-3/7 enzymatic activity. Activation of caspase-3/7 releases rhodamine 110, which emits fluorescence. The intensity of fluorescence was measured (Fluoroskan Ascent, Labsystems, Helsinki, Finland) using an excitation wavelength of 485 nm and an emission wavelength of 538 nm. The fluorescence intensity was expressed as raw fluorescence intensity units after subtraction of background fluorescence intensity.

Measurement of LDH concentrations

LDH concentrations in the culture supernatants were measured as described by Amador *et al.*[25]

Statistical analysis

Results are expressed as mean ± SEM. Statistical analysis was performed by one-way ANOVA using Stat View v5.0 (SAS Institute Inc., Cary, NC, USA). For all analyses, values of $P < 0.05$ were considered significant. In the experiments with cultures of human tracheal epithelial cells, *n* refers to the number of donor tracheae from which cultured epithelial cells were derived.

RESULTS

Assessment of DNA fragmentation and cell death

Levels of DNA fragmentation in the cells as assessed by the cell death detection ELISA were low after 72 h of pretreatment with L-carbocisteine or vehicle (ddH_2O) (Fig. 1a), and also 12 and 24 h after exposure to H_2O_2 vehicle (0.1% ddH_2O) (Fig. 1a). Likewise, DNA fragmentation in the cells treated with 0.1% ddH_2O at

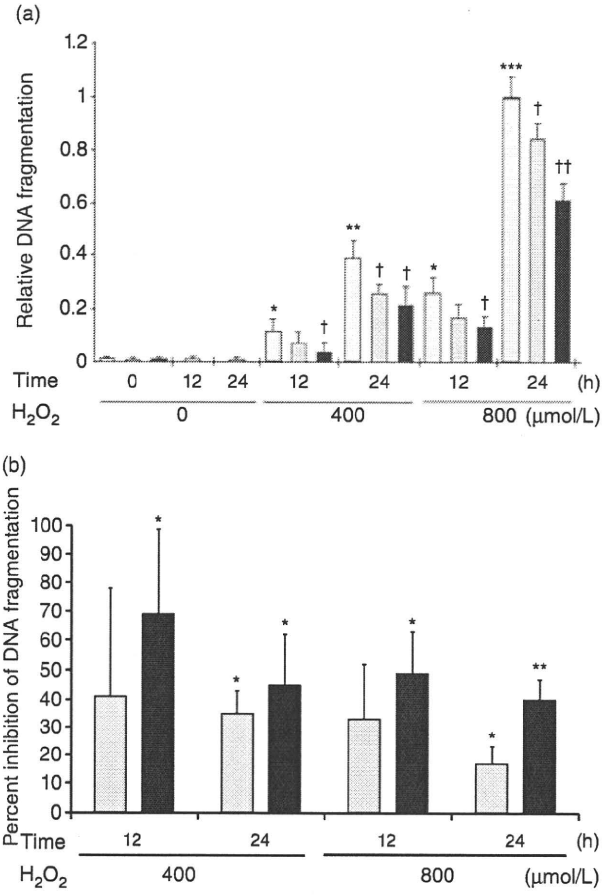

Figure 1 (a) Effects of L-carbocisteine (1 or 10 μmol/L) on relative DNA fragmentation in primary cultures of human tracheal epithelial cells 12 or 24 h after treatment with H_2O_2 (400 and 800 μmol/L) or vehicle (0.1% ddH_2O). DNA fragmentation 24 h after stimulation with H_2O_2 (800 μmol/L) in the presence of vehicle was set at 1.0 and all other measurements were normalized to the control values for the purposes of comparison. Results are mean ± SEM from five samples. Significant differences from values before pretreatment with L-carbocisteine (time 0) are indicated as $^*P < 0.05$, $^{**}P < 0.01$ and $^{***}P < 0.001$. Significant differences from values after treatment with H_2O_2 at each time point are indicated as $^{+}P < 0.05$ and $^{++}P < 0.01$. (b) Percent inhibition of DNA fragmentation by L-carbocisteine (1 or 10 μmol/L) compared with DNA fragmentation after vehicle (0.1% ddH_2O) in primary cultures of human tracheal epithelial cells, 12 or 24 h after treatment with H_2O_2 (400 and 800 μmol/L). Results are mean ± SEM from five samples. Significant differences from values after exposure to H_2O_2 and vehicle (0.1% ddH_2O), at each time point and H_2O_2 concentration, are indicated as $^*P < 0.05$ and $^{**}P < 0.01$. (□) Vehicle (0.1% ddH_2O), (▨) H_2O_2 + 0.1% ddH_2O, (▣) carbocisteine (1 μmol/L), (■) carbocisteine (10 μmol/L).

12 and 24 h was not different compared with that before treatment (Fig. 1a). In preliminary experiments, H_2O_2 induced DNA fragmentation in a narrow range of concentrations between 400 and 800 μmol/L. Therefore, to examine the dose–response effects of H_2O_2 on the viability of the human tracheal epithelial cells, the cells were treated with 400 and 800 μmol/L H_2O_2. H_2O_2 (400 or 800 μmol/L) caused a significant increase in DNA fragmentation at 12 and 24 h. The effects of H_2O_2 on the levels of DNA fragmentation in human tracheal epithelial cells depended on concentration and the incubation period ($P < 0.05$). L-carbocisteine (10 μmol/L) significantly inhibited H_2O_2-induced DNA fragmentation (Fig. 1a) by 69% (400 μmol/L) and 49% (800 μmol/L) at 12 h (Fig. 1b), and by 45% (400 μmol/L) and 40% (800 μmol/L) at 24 h of exposure to H_2O_2 (Fig. 1b). Likewise, 1 μmol/L L-carbocisteine significantly inhibited H_2O_2-induced DNA fragmentation by 35% (400 μmol/L) and 17% (800 μmol/L) at 24 h of exposure to H_2O_2 (Fig. 1b).

The total number of viable cells and the viability of cells from a patient with prostate cancer complicated by COPD were not different compared with those from patients without COPD (data not shown). Levels of DNA fragmentation induced by H_2O_2 and the inhibitory effects of L-carbocisteine in cells from a COPD patient were not different from those in cells from patients without COPD (data not shown). LDH concentrations in supernatants before and after exposure to H_2O_2 were low (<10 IU/L) (data not shown).

Assessment of caspase-3 and caspase-9 activation

A band for non-cleaved caspase-3 was consistently observed by western blot analysis of human tracheal epithelial cells before exposure to H_2O_2 (800 μmol/L). In contrast, the band for cleaved caspase-3 was not observed before exposure to H_2O_2. The intensity of the band for non-cleaved caspase-3 did not change, while the intensity of the band for cleaved caspase-3 increased, 8 h after exposure to H_2O_2. Treatment of the cells with L-carbocisteine (10 μmol/L) reduced the intensity of the band for cleaved caspase-3, 8 h after exposure to H_2O_2 (800 μmol/L), by more than 50% compared with that for cells treated with vehicle (Fig. 2). In contrast, L-carbocisteine (10 μmol/L) increased the intensity of the non-cleaved caspase-3 band.

Likewise, the band for non-cleaved caspase-9 was observed, whereas that for cleaved caspase-9 was not observed in the cells before exposure to H_2O_2. The intensity of the band for cleaved caspase-9 increased, while the band for non-cleaved caspase-9 was not observed, 8 h after exposure to H_2O_2. Treatment of the cells with L-carbocisteine (10 μmol/L) reduced the intensity of the band for cleaved caspase-9, 8 h after exposure to H_2O_2 (800 μmol/L), by more than 90% compared with that for cells treated with vehicle (Fig. 3). On the other hand, L-carbocisteine (10 μmol/L) increased the intensity of the non-cleaved caspase-9 band.

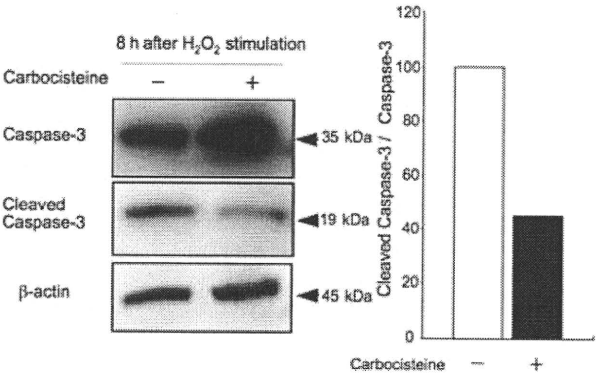

Figure 2 (Left) Western blot analysis of cleaved and non-cleaved caspase-3 and β-actin in human tracheal epithelial cells, 8 h after exposure to H_2O_2 (800 μmol/L) in the presence of L-carbocisteine (10 μmol/L) (+) or vehicle (0.1% ddH_2O) (–). Data are representative of five separate experiments. (Right) The intensity of the cleaved and non-cleaved caspase-3 bands in a representative experiment performed 8 h after exposure to H_2O_2 (800 μmol/L) in the presence of L-carbocisteine (10 μmol/L) (+) or vehicle (0.1% ddH_2O) (–). The ratio of cleaved/non-cleaved caspase-3, 8 h after exposure to H_2O_2 in the presence of vehicle (0.1% ddH_2O) was set at 100. The intensity of the cleaved caspase-3 band was reduced in the presence of L-carbocisteine. (□) Vehicle (0.1% ddH_2O), (■) carbocisteine (10 μmol/L).

Caspase-3 activity

Caspase-3 activity, as measured using a fluorescent detection kit, was also consistently observed in cultured human tracheal epithelial cells in the absence of H_2O_2 (Fig. 4). Pretreatment with L-carbocisteine (1 or 10 μmol/L) did not change caspase-3 activity before H_2O_2 exposure. Exposure to H_2O_2 (800 μmol/L, 8 h) increased caspase-3 activity, and L-carbocisteine (10 μmol/L) inhibited the increase in caspase-3 activity induced by H_2O_2 (Fig. 4).

Assessment of Akt activation

Akt and phospho-Akt, as measured by western blot analysis, were consistently observed in cultured human tracheal epithelial cells before exposure to H_2O_2 (Fig. 5, left). L-carbocisteine (10 μmol/L) did not change Akt levels before H_2O_2 exposure. In contrast, L-carbocisteine (10 μmol/L) increased the phospho-Akt levels (Fig. 5, left), and the ratio of phospho-Akt/Akt by 60% (Fig. 5, right). Akt and phospho-Akt levels decreased 8 h after exposure to H_2O_2 in cells treated with vehicle (data not shown). After exposure to H_2O_2, L-carbocisteine (10 μmol/L) did not change phospho-Akt levels (data not shown), while Akt levels increased in the cells treated with vehicle (data not shown).

Effects of Akt inhibitors on DNA fragmentation

To examine the role of Akt in the inhibitory effects of L-carbocisteine on DNA fragmentation induced by